QUANTUM FLUORESCENCE EFFICIENCIES OF MARINE FULVIC AND HUMIC ACIDS

by

STEVEN K. HAWES

skh@monte.marine.usf.edu

A thesis submitted in partial fulfillment of the
requirements for the degree of Master of Science

Department of Marine Science
University of South Florida

December 1992

Major Professor: Kendall L. Carder, Ph.D.

ACKNOWLEDGEMENTS

I wish to express my gratitude for the support and patience of Dr. Kendall Carder. This thesis could not have come about without his ideas, advice, time, and energy.

Thanks are also due to Bob Steward and Joan Hesler for their continuous assistance, to Dr. Edward Van Vleet and Dr. Robert Byrne for their scholarly advice and generous donation of lab facilities, to Dr. George Harvey for donating humic materials, and to Tom Peacock and Zhongping Lee for insightful discussions. Financial support was provided by NASA through grant NAEW-465 and GSFC contract NAS5-30779, and by ONR through grant N00014-89-J-1091. Ship support was provided by the State of Florida through the Florida Institute of Oceanography.

My deepest gratitude goes out to my father, Ray Hawes, who taught me to think, and to my mother, Alice Hawes, who taught me to love.

TABLE OF CONTENTS

LIST OF TABLES

LIST OF FIGURES

LIST OF SYMBOLS

a	absorption coefficient, m^{-1}
a^*	mass-specific absorption coefficient, m^2/mg or m^2/g
a'	measured absorption calculated with CDOM fluorescence effects included, m^{-1}
A	absorbance, dimensionless
A'	measured absorbance calculated with CDOM fluorescence effects included, dimensionless
A_0	parameter for $\eta(\lambda_x,\lambda_m)$ model, nm^{-1}
A_1	parameter for $\eta(\lambda_x,\lambda_m)$ model, dimensionless
A_2	parameter for $\eta(\lambda_x,\lambda_m)$ model, dimensionless
b_b	backscattering coefficient, m^{-1}
B_1	parameter for $\eta(\lambda_x,\lambda_m)$ model, nm^{-1}
B_2	parameter for $\eta(\lambda_x,\lambda_m)$ model, nm^{-1}
C	concentration, mg/m^3 or g/m^3
CDOM	colored, dissolved organic matter
<Chl *a*>	chlorophyll *a* concentration, mg/m^3
CZCS	Coastal Zone Color Scanner
D	distribution function, dimensionless
DIW	de-ionized water

DOC	dissolved organic carbon
DOM	dissolved organic matter
E	irradiance, quanta/area-time-nm
$E_d(0-)$	downwelling irradiance just below the sea-surface, quanta/area-time-nm
EEM	fluorescence excitation-emission matrix
f	fulvic acid fraction of total humus
F	measured fluorescence intensity, quanta/time-steradian
F_c	measured fluorescence intensity corrected for instrumental sensitivity, quanta/time-steradian
FA	fulvic acid
HA	humic acid
I	instrumental constant for airborne fluorometer
K	diffuse attenuation coefficient, m^{-1}
l	pathlength, m
L	radiance, quanta/area-time-steradian-nm
L_w	water-leaving radiance, quanta/area-time-steradian-nm
m	total recovered mass, mg
n	number of data points
NIST	National Institute of Standards and Technology
<pheo *a*>	pheophytin *a* concentration, mg/m^3
P	pigment concentration = <Chl *a*> + <pheo *a*>, mg/m^3
P_{alg}	P calculated via CZCS-type spectral ratio algorithm
P'_{alg}	P_{alg} calculated with CDOM fluorescence effects included

q	spectral correction factor for spectrofluorometer
QSD	quinine sulfate dihydrate
r	backscattering shape factor, dimensionless
r^2	correlation coefficient
R	reflectance = E_u/E_d, dimensionless
R_{rs}	remote-sensing reflectance = L_w/E_d, steradians^{-1}
REC	recovery efficiency for humus, dimensionless
Rubipy	Tris(2,2'-bipyridyl)ruthenium(II) chloride hexahydrate
S	spectral slope of CDOM, FA, or HA absorption spectrum, nm^{-1}
Sea-WiFS	Sea-viewing, Wide Field-of-view Sensor
T	transmittance, dimensionless
v	total volume of water sampled, liters
x	distance along reflecting tube cylinder, m
η	spectral quantum fluorescence efficiency function, nm^{-1}
θ	angle relative to zenith or relative to normal, degrees
θ_{max}	maximum angle of collection, degrees
λ	wavelength, nm
μ	average of $\cos\theta_n$ for n photons
ν	wavenumber, cm^{-1}
$\Delta\nu$	approximate width at half-maximum for Gaussian curve, cm^{-1}
σ_n	standard deviation
Φ_f	quantum fluorescence efficiency, dimensionless

ω	solid angle, steradians

FOR SYMBOLS	SUBSCRIPTS
a, a^*, A, b_b, C, S, T, η, and Φ_f	cdom, f, h, p, and w refer to CDOM, FA, HA, particles, and water
λ, ν	x, m, and 0 refer to excitation, emission, and wavenumber of maximum emission
D, E, K, L, r, R	d, f, and u refer to downwelling, originating from CDOM fluorescence, and upwelling

QUANTUM FLUORESCENCE EFFICIENCIES OF MARINE FULVIC AND HUMIC ACIDS

by

STEVEN K. HAWES

An Abstract

Of a thesis submitted in partial fulfillment of the requirements for the degree of Master of Science

Department of Marine Science
University of South Florida

December 1992

Major Professor: Kendall L. Carder, Ph.D.

Fluorescence due to CDOM (colored, dissolved orgainc matter; also gelbstoff) in the ocean has long been observed, but the quantitative measures of such fluorescence that are needed in optical models are few. Here, quantum fluorescence efficiencies ($\Phi_f(\lambda_x)$ = quanta fluoresced at all λ_m per quanta absorbed at λ_x, λ_x = excitation wavelength, λ_m = emission wavelength) and spectral fluorescence efficiency functions ($\eta(\lambda_x,\lambda_m)$ = quanta fluoresced per nanometer interval of λ_m per quanta absorbed at λ_x) have been determined for 4 fulvic acid and 7 humic acid samples that have been isolated from diverse marine environments. The $\eta(\lambda_x,\lambda_m)$ functions have been described mathematically. These data are used to examine the effect of solar-stimulated CDOM fluorescence on ocean color remote sensing, to examine some aspects of using fluorometry to quantify CDOM, and to examine the effect of CDOM fluorescence on absorption measurements of natural water samples made using both diode array spectrophotometers and reflecting tube absorption meters. CDOM fluorescence causes less than a 5% overestimate in remotely sensed (e.g. via the Coastal Zone Color Scanner) phytoplankton pigment concentrations for a transect off Tampa Bay, Florida. CDOM fluorescence has no affect on measurements made using diode array spectrophotometers, but it can cause a small but detectable lowering of measurements made using reflecting tube absorption meters.

Abstract approved: _____

Major Professor: Kendall L. Carder, Ph.D.
Professor, Department of Marine Science

Date approved: _____

INTRODUCTION

Dissolved organic matter (DOM) represents the largest pool of organic carbon in the oceans (600-1700 x 10^{15} g C compared to 2 x 10^{15} g C for oceanic biota; Aiken et al., 1985; Hedges et al., 1992). It plays an important role in the global carbon cycle, and it may be important for oceanic mitigation of atmospheric $C0_2$ buildup (Toggweiler, 1989; Bacastow and Maier-Reimer, 1991; Walsh et al., 1992). It affects many geochemical and biological reactions throughout the water column (Pocklington, 1977; Horth et al., 1988; Mueller-Wegener, 1988), and by absorbing sunlight it initiates many photochemical reactions in the surface layers (Zepp and Schlotzhauer, 1981; Zika, 1981; Zepp, 1988; Leifer, 1988). The ubiquitous distribution of DOM in natural waters makes it an important object of study in many oceanographic disciplines.

DOM is also of major interest in optical oceanography because it absorbs strongly in blue and UV wavelengths, and it fluoresces in the blue to blue-green region. The fraction of DOM that absorbs light can be called colored DOM, or CDOM (also gelbstoff or yellow substance). This absorption has been used to provide an estimate of DOM concentrations (Lewis and Canfield, 1977; references cited in Zepp and Schlotzhauer, 1981) and as a measure of the reaction rate for CDOM-sensitized photolysis of pollutants (Zepp and Schlotzhauer, 1981; Leifer,

1988). Other studies have established that CDOM absorption can significantly affect the spectral light field in the ocean and that it must be accounted for in many ocean color remote sensing applications (Bricaud et al., 1981; Prieur and Sathyendranath, 1981; Morel, 1988; Gordon et al., 1988; Carder et al., 1989; Carder et al., 1991). For example, CDOM absorbs more blue light (443 nm) than green light (550 nm), just as phytoplankton does, but it does not necessarily covary with phytoplankton. Thus, phytoplankton pigment algorithms such as the one developed for the Coastal Zone Color Scanner (CZCS) which use radiance measurements at 443 nm and 550 nm (Gordon and Morel, 1983) cannot distinguish between CDOM and phytoplankton. However, Carder et al. (1991) have shown that the absorption characteristics can be used to both differentiate CDOM from phytoplankton pigments and estimate its concentration by utilizing an additional radiance measurement at 412 nm. CDOM absorption measurements from space will thus soon be possible with the launch of the Sea-viewing Wide Field-of-view Sensor (Sea-WiFS) in 1993, which will detect radiance at 412, 443, and 565 nm, and at three other visible and two infrared bands.

CDOM fluorescence has also been studied intensely for decades, being utilized as a tracer for water masses (Laane, 1981; Berger et al., 1984; Willey, 1984; Cabaniss and Shuman, 1987), as a measure of organic carbon (Black and Christman, 1963; Smart et al., 1976; Ferrari and Tassan, 1991), and as a means of characterizing DOM (Stewart and Wetzel, 1980, 1981; Ewald et al., 1983; Hayase and Tsubota, 1985; Donard et al., 1989; Coble et al., 1990, 1992; Coble, 1992). These studies for the most part measure CDOM fluorescence in terms of relative fluorescence intensity,

or at best as "millifluorescence units" (Kalle, 1963). However, in order to include this fluorescence in oceanic optical models, or to calculate its effect on other optical properties, quantitative measurements are needed. For instance, CDOM fluorescence may be a significant portion of the upwelling radiance at the surface of the ocean (Spitzer and Dirks, 1985), which is the optical quantity detected by overflying remote sensors. Also, Monte Carlo models of the light field in the ocean (Poole and Esaias, 1981; Gordon, 1985, 1989; Stavn and Weidemann, 1989; Stavn, 1990), which model individual photon paths based on the optical properties of the water column, need to incorporate the possibility of fluorescence when a photon is absorbed by CDOM, or else determine that CDOM fluorescence is negligible compared to the other photon fluxes. Both of these problems require quantitative descriptions of CDOM fluorescence as input to the models. In addition, fluorometric methods for measuring CDOM concentrations will be enhanced by gaining quantitative knowledge of CDOM fluorescence properties.

The only truly quantitative measures of CDOM fluorescence to date are are those of Zepp and Shlotzhauer (1981) who reported the fluorescence quantum efficiencies (Φ_f) for numerous terrestrial and riverine humic substances for excitation at 350 nm, where $\Phi_f(\lambda_x)$ is defined as the number of quanta fluoresced by a substance at all emission wavelengths (λ_m) divided by the quanta absorbed at the excitation wavelength, λ_x. However, these data are inadequate for many optical modeling applications because the spectral character of the emission has been lost by integration, and many applications require excitation at wavelengths other than 350

nm. To properly model CDOM fluorescence the "spectral fluorescence efficiency function," $\eta(\lambda_x,\lambda_m)$, for CDOM must be determined. $\eta(\lambda_x,\lambda_m)$ is defined as the number of quanta fluoresced per nm interval of λ_m divided by the quanta absorbed at λ_x. $\eta(\lambda_x,\lambda_m)$ combined with the CDOM absorption coefficient represents one component of the inelastic or transpectral scattering coefficient (Gordon, 1979; Preisendorfer and Mobley, 1988), which is, along with the absorption and volume scattering coefficients, one of the "inherent optical properties" of natural waters - an optical property that is independent of the ambient light field (Kirk, 1983). Other major components of the inelastic scattering coefficient are water Raman scattering and fluorescence from phytoplankton pigments, neither of which will be examined here.

Although the exact chemical structure of the absorbing and fluorescing chromophores in CDOM remains controversial (Harvey et al., 1983; Laane, 1984; Harvey, 1984; Coble et al., 1990, 1992; Coble, 1992), it is widely believed that humic substances (also humus), specifically fulvic acid (FA) and humic acid (HA), are largely responsible for this absorption, and thus for the fluorescence as well (Zepp and Schlotzhauer, 1981; Carder et al., 1989). Humic substances are high molecular weight organic acids that conform to no specific chemical structure, and recent elemental, $\delta^{13}C$, and ^{13}C-NMR analyses indicate that marine humic substances differ markedly from riverine humic substances, suggesting that they have a marine phytoplanktonic source (Hedges et al., 1992). By definition, FA is the fraction of the humus that is soluble at all pH values and HA is the fraction that is soluble above pH

2 but insoluble at or below pH 2, and together, FA and HA represent 10%-60% of the total oceanic pool of DOM (Harvey et al., 1983; Aiken, 1985). As general compound classes, FA and HA exhibit optical properties different from each other, but these properties are relatively homogenous within each class. Both the mass-specific absorption coefficient and the spectral slope (the slope of the absorption spectrum plotted with a logarithmic ordinate) have been found to differ for FA versus HA for marine, sedimentary, and terrestrial environments (Carder et al., 1989; Hayase and Tsubota, 1985; Zepp and Schlotzhauer, 1981, respectively). In addition, limnological data have been published that suggest that lacustrine FA and HA have different Φ_f values (Stewart and Wetzel, 1980; Carlson and Shapiro, 1981). Since the ratio of FA to HA is variable in natural waters (Stuermer, 1975; Harvey et al., 1983; Carder et al., 1989), optical models that account for both of these constituents separately will be better able to resolve CDOM optical properties than will models that account for CDOM as a single parameter. In this paper, it will be assumed that FA and HA comprise the sum total of CDOM, although there are certain conditions where this approximation may become invalid - in phytoplankton blooms with high levels of dissolved pigments in the water column, for example. CDOM absorption or fluorescence calculated from the sum of the corresponding measured properties of FA and HA can only be underestimated using this assumption.

The remainder of this paper is divided into two parts. In Part 1, both $\Phi_f(\lambda_x)$ and $\eta(\lambda_x,\lambda_m)$ are determined for an array of excitation wavelengths for several different FA and HA samples that have been isolated from diverse marine

environments, using both quinine sulfate dihydrate (QSD) and Tris(2,2'-bipyridyl)ruthenium(II) chloride hexahydrate (Rubipy) as fluorescence standards. The $\eta(\lambda_x,\lambda_m)$ measurements for each sample are represented by mesh surface plots, and they have been modeled mathematically for easy incorporation into optical models.

In Part 2, the fluorescence efficiency measurements are applied to 3 optical problems. First, the effect of solar-induced CDOM fluorescence on surface irradiance reflectance is investigated using a simple radiative transfer model and a previously published model. Second, some aspects of using fluorometry to quantify CDOM are discussed in light of the $\eta(\lambda_x,\lambda_m)$ measurements. Third, the data are used to assess the impact of CDOM fluorescence on absorption measurements made using diode array spectrophotometers and reflecting tube absorption meters.

PART 1: CALCULATION OF $\Phi_f(\lambda_x)$ AND $\eta(\lambda_x,\lambda_m)$ FOR FA AND HA

Materials

Recovery of humic substances from seawater

The FA and HA samples investigated were isolated from several different sites, including the Peruvian upwelling area, a variety of sites in the Gulf of Mexico, and the North Atlantic. Two samples were obtained from Dr. George Harvey (NOAA/AOML), and the others were isolated using either XAD-2 macroreticular sorbent (from Rohm and Haas) or C_{18} reverse-phase sorbent (from Varian). Sampling and recovery information is listed in Table 1.

The procedure for isolation of humic substances using XAD-2 closely followed that described in Harvey et al. (1983). The resin was cleaned by refluxing in an MeOH:toluene azeotrope for 6 hrs. and was secured in a 1.5 cm x 22 cm glass column (column geometries in this paper refer to inside diameter x length) with pre-combusted glass wool plugs above and below. Seawater was sampled using a 30 l Go-flo bottle fitted with a Teflon-lined spring, and then acidified to a pH of about 2 in a stainless steel resevoir. Humic substances were extracted by passing the water through the column at a flow rate of about 20 ml/min. The columns were rinsed with

Table 1. FA and HA sampling and recovery information. Samples HA1 and HA2 were obtained from Dr. George Harvey and some information for these samples in not available.

sample name	location	sample date	sample volume (liters)	extraction method	tot. mass recovered (mg)
HA1	Peru upwelling (El Nino)	-	-	XAD2	-
HA2	Gulf of Mexico, outside Loop Cur.	-	-	XAD2	-
HA4	Gulf of Mexico, mouth of Tampa Bay	12oct89	26	XAD2	0.156
HA5	Gulf of Mexico, within Loop Cur.	15oct89	57	XAD2	0.004
HA6	Gulf of Mexico, mid-West Florida Shelf	04mar90	55	XAD2	0.65
FA7	Gulf of Mexico, mid-West Florida Shelf	04mar90	32	C18	12.66
FA8 HA8	Gulf of Mexico, mouth of Tampa Bay	05mar90	20	C18	2.24 0.42
FA9	North Atlantic 60°N 20°W	24may91	55	C18	19.06
FA11 HA10	North Atlantic 60°N 20°W	20aug91	55	C18	6.99 ≈ 0

de-ionized water (DIW) to remove salts, and humic substances were eluted with ≈ 170 ml of either 1.0 N NH_4OH or 1.0 N NH_4OH in MeOH (pH ≈ 11.1). The flow rate for elution was 2-4 ml/min. The eluate was concentrated by rotary evaporation (driving off the ammonia and MeOH and leaving the humus in aqueous solution), extracted with CH_2Cl_2 to remove lipids, acidified to a pH of about 2, and set in the refrigerator for 2 days. By definition, HA precipitates at pH 2 and FA remains in solution. The solution was centrifuged, the FA solution pipetted out, and both fractions were freeze-dried to yield solid FA and HA.

Four of the samples were isolated using Mega Bond Elut C_{18} cartridges from Varian. Procedures were adapted with slight variations from Amador et al. (1991). Seawater was sampled in the same way as for the XAD-2 procedure. Two general isolation schemes were tried, with slight variations within each scheme.

Scheme 1, Samples 7 and 8: C_{18} cartridges containing 5 g of sorbent were pre-treated with 10 ml 0.3 mM HCl, 50 ml MeOH, and 50 ml DIW. Each seawater sample was acidified to pH 2.5 and pulled through a 0.2 uM pore diameter Gelman filter cartridge and 2 C_{18} cartridges in line at a flow rate of about 20-30 ml/min using a peristaltic pump. Each C_{18} cartridge was eluted sequentially with 15 ml each of DIW, 25 mM $NaHCO_3$, DIW, MeOH, 25 mM $NaHCO_3$, DIW, and a final MeOH rinse. 4 MeOH eluants per sample (2 from each cartridge) were combined and concentrated to ≈ 10 ml by rotary evaporation at < 40°C. The other eluants were discarded. A whitish precipitate formed during evaporation which was centrifuged out and discarded (see Appendix 1). The supernatant was washed with CH_2Cl_2 to

remove lipids, acidifed to a pH of about 2, and set in the refrigerator overnight allowing HA precipitation. The solutions were then centrifuged, the FA fraction pipetted out, and both fractions were freeze dried. No HA precipitated from Sample 7, and some HA may have been lost when the whitish precipitate was discarded.

Scheme 2, Samples 9, 10, and 11: C_{18} cartridges containing 10 g of sorbent were pre-treated with 50 ml MeOH and 50 ml DIW. Each seawater sample was acidified to pH 2 and pulled thru a 0.2 uM pore diameter Gelman filter cartridge and 2 C_{18} cartridges as in Scheme 1. Each cartridge was washed with 50 ml of DIW, 25 ml of 1.0 N NH_4OH in MeOH, and 25 ml of MeOH. An additional 25 ml of either MeOH or NH_4OH/MeOH was drawn through the upstream cartridge i.e. the cartridge with most of the extracted humic substances. All MeOH and NH_4OH/MeOH eluants were combined and processed as the MeOH eluants from Scheme 1. Very little HA precipitated from any of these samples.

Reconstitution of isolated samples

Aqueous FA and HA solutions were prepared by weighing out fractions of the freeze-dried solids, dissolving initially in a couple of drops of strong NaOH, quickly diluting with a bicarbonate-buffered artificial seawater (Salinity = 28.7, pH = 8.3 to 8.5; adapted from Kester et al., 1967), and adding enough strong HCl to neutralize the initial NaOH. Values of pH for the final solutions ranged from 7.8 to 8.3, and concentrations ranged from 64 to 304 mg/l for the FA samples and from 13.1 to 30

mg/l for the HA. In several of the solutions small particles were present, possibly due to incomplete dissolution, or from dust or some other contaminant in the solids. Solutions were centrifuged to remove these particles and pipetted into a 1 cm pathlength, Teflon-stoppered, quartz cuvette for the optical measurements. The same cuvette was used for all optical measurements. FA and HA solutions were not degassed, as Zepp and Schlotzhauer (1981) found that degassing a water sample from the Aucilla River, Florida, did not affect the fluorescence efficiency of the sample. Reconstituted sample information is listed in Table 2.

Standard dye solutions

QSD was obtained from the National Institute of Standards and Technology (NIST). QSD was dissolved in 0.105 N $HClO_4$ and was not degassed since oxygen quenching of QSD fluorescence is negligible (Velapoldi and Mielenz, 1980). The concentration was 3.83 uM and the solution was transferred to the cuvette with a glass pipette.

Rubipy was obtained from Aldrich Chemical Co. Rubipy was dissolved in DIW and de-oxygenated by bubbling N_2 into the solution for at least 20 minutes, since oxygen quenches Rubipy fluorescence (Van Houten and Watts, 1976). The concentration was 2.14 uM and the de-oxygenated solution was transferred to the cuvette with a glass syringe using a technique that prevents re-aeration of the solution during transfer. Briefly, 5 ml of de-aerated solution is drawn into the syringe, the

Table 2. Reconstituted FA and HA absorption parameters. FA and HA solutions were made from sub-fractions of the total recovered masses listed in Table 1. S is calculated by linear regression on $\ln(a_{cdom}(\lambda))$, roughly in the range of 350 nm $< \lambda <$ 550 nm. r^2 is the correlation coefficient and n is the number of points sampled for the regression. A short dash (-) indicates that no data is available.

THIS STUDY: sample name	conc. (mg/l)	a*(350) (m^2/g)	S (nm^{-1})	r^2	n
FA7	223	0.042	0.0162	0.999	11
FA8	64	0.331	0.0160	0.998	22
FA9	279	0.073	0.0155	0.999	17
FA11	304	0.065	0.0151	0.999	17
avg. FA		0.060[a]	0.0156		
HA1	13.1	0.663	0.011	-	-
HA2	17.5	0.283	0.0142	0.999	23
HA4	-	-	0.0122	0.998	21
HA5	-	-	0.0131	0.993	13
HA6	30.0	0.220	0.0130	0.998	21
HA8	21.0	0.311	0.011	0.999	22
HA10	-	-	0.0212	0.998	15
avg. HA		0.419	0.0124[b]		

OTHER STUDIES: sample type	a*(350) m^2/g	S 1/nm	source
CDOM	-	0.014	global[c]
soil FA	1.59	0.0138	various soils[d]
soil HA	2.44	0.0102	"
CDOM	1.51	0.0145	various freshwaters[d]
CDOM	-	0.014	Baltic Sea[e]
FA	0.031	0.0184	GOM Loop Current[f]
HA	0.391	0.011	"
CDOM	-	0.0140	Orinoco River outflow[g]

[a]a*(350) for FA8 excluded from average; [b]S for HA10 excluded from average; [c]Bricaud et al., 1981; [d]Zepp and Schlotzhauer, 1981; [e]Hojerslev, 1988; [f]Carder et al., 1989; [g]Blough et al., 1991.

syringe is inverted, and 4 ml of solution is purged, leaving 1 ml. Solution is again drawn up to 5 ml and the syringe is inverted and purged as before. Solution is again drawn up to 5 ml and the entire contents is purged into the cuvette. Since the cuvette holds about 3 ml, the first 2 ml of solution flows up and out of the cuvette which is then quickly stoppered.

Measurements

All solutions were kept in the dark as much as possible, and at no time were any of them exposed to the room lighting for more than about a minute. This should lead to negligible photo-bleaching of either absorbance or fluorescence (Kouassi, 1986). The ranges of pH (7.8-8.3) and temperature (room temperature ranged from around 22-26 °C) for the FA and HA solutions should lead to changes in absorption and fluorescence of only a few percent (Smart et al., 1976; Stewart and Wetzel, 1980; Carlson and Shapiro, 1981; Visser, 1983).

Absorbance measurements

Absorbances of the FA, HA, QSD, and Rubipy solutions in the 1 cm pathlength cuvette were determined on a Cary 2200 spectrophotometer. Absorbance was determined at 10 discrete wavelengths ranging from 310 nm to 490 nm at 20 nm increments for the FA, HA, and Rubipy solutions, and at 5 discrete wavelengths

ranging from 310 nm to 390 nm for the QSD solution, since QSD does not absorb beyond 400 nm. For the FA and HA solutions, additional absorbance measurements were taken out to 700 nm. The spectral bandwidth was 3 nm. Dilutions were made as necessary to keep absorbances < 0.05 at all wavelengths. Measured absorbance was corrected point-by-point by subtracting the absorbance of the appropriate solvent.

Fluorescence emission spectra

Fluorescence emission spectra were determined on a Perkin-Elmer LS-5 Luminescence spectrophotometer directly after the absorbance measurements were obtained, using the same solutions in the same cuvette. Emission spectra were measured for ten different λ_x for each solution (five for the QSD), corresponding to those wavelengths at which absorbance was measured. λ_m was scanned from (λ_x+10) to 700 nm for the FA, HA, and QSD solutions, and from 520 to 800 nm for the Rubipy solution. The excitation slit width was set to 3 nm to correspond with that used for the absorbance measurements, and the emission slit width was opened wider to 10 nm to increase the signal-to-noise ratio. Fluorescence was measured every 0.5 nm at a scan rate of 1 nm/sec. Appropriate solvent blanks were subtracted point-by-point from each spectrum and the outputs were averaged into 5 nm bins.

The resulting spectra were corrected for varying instrumental sensitivity with respect to λ_m by the method described in Velapoldi and Mielenz (1980). Briefly, the fluorescence emission spectrum of a 1.28 uM solution of QSD in 0.105 N $HClO_4$ is

measured (= $F_{q,meas}(\lambda_m)$) and divided by the absolute photon spectrum of QSD determined by NIST (= $F_{q,nist}(\lambda_m)$) yielding correction factors $q(\lambda_m)$, i.e.

$$q(\lambda_m) = \frac{F_{q,meas}(\lambda_m)}{F_{q,nist}(\lambda_m)} \quad (1)$$

Any emission spectrum measured using the same configuration on the same spectrofluorometer can be corrected by dividing through point-by-point by $q(\lambda_m)$, yielding an ordinate that is scaled in relative quanta fluoresced per unit time.

$q(\lambda_m)$ is determined in the above manner for λ_m = 375-675 nm, the limits of the NIST spectrum. For the 320-375 nm and 675-800 nm ranges, $q(\lambda_m)$ was approximated by extrapolating the measured correction curve with a quadratic and an exponential fit, respectively (see Figure 1). For $\lambda_x > 300$ nm, very little fluorescence occurs outside the 375-675 nm emission range for FA, HA, and QSD. Thus errors in calculated total fluorescence (i.e. integrated over λ_m) associated with using the extrapolated $q(\lambda_m)$ factors for these solutions is negligible. In addition, the calculated ratio of $\Phi_f(\lambda_x)$ for the Rubipy and QSD solutions were found to agree closely to the ratio of published values, so the error using the extrapolated $q(\lambda_m)$ values for Rubipy is also small, even though a significant fraction of the Rubipy fluorescence occurs at $\lambda_m > 675$ nm (see Figure 1).

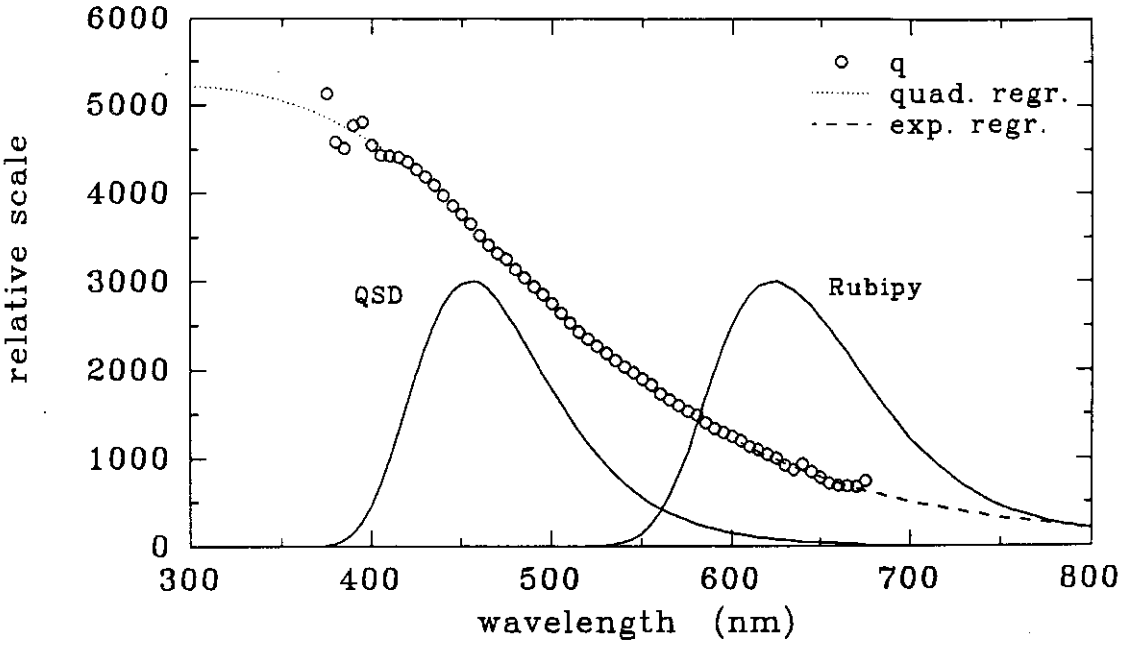

Figure 1. Spectral correction factors, q(λ), for the spectrofluorometer used in this study, determined by the method of Velapoldi and Mielenz (1980). The short wavelength end is extended by a quadratic fit and the long wavelength end by an exponential fit. Also shown are fluorescence emission curve shapes for QSD and Rubipy.

Calculation of $\Phi_f(\lambda_x)$

$\Phi_f(\lambda_x)$ is calculated using the equation

$$\phi_{f,i}(\lambda_x) = \phi_{f,std}(\lambda_x) \frac{a_{std}(\lambda_x)}{a_i(\lambda_x)} \frac{\int F_{c,i}(\lambda_x,\lambda_m)\, d\lambda_m}{\int F_{c,std}(\lambda_x,\lambda_m)\, d\lambda_m} \quad (2)$$

where $a(\lambda_x)$ = the absorption coefficient = 2.303 $A(\lambda_x)/l$ in m^{-1}, $A(\lambda_x)$ is the absorbance, l is the pathlength in meters, and $F_c(\lambda_x,\lambda_m)$ is the fluorescence intensity corrected by the method described in the preceeding section in units of relative quanta per unit time. The subscript 'i' refers to any FA or HA sample and the subscript 'std' refers to a fluorescence standard of known Φ_f, here either QSD or Rubipy. QSD has a quantum yield, $\Phi_{f,q}(\lambda_x)$, of 0.59 in 0.105 N $HClO_4$ for λ_x = 220-390 nm (Velapoldi and Mielenz, 1980). Rubipy has a quantum yield, $\Phi_{f,r}(\lambda_x)$, of 0.042 in water for λ_x = 436 nm (Van Houten and Watts, 1976), and it was assumed to be constant for λ_x = 310-490 nm. According to R.J. Watts (personal communication), this assumption is probably valid. Also, since the calculated ratio $\Phi_{f,q}(\lambda_x):\Phi_{f,r}(\lambda_x)$ was found to agree with the ratio of published values for λ_x = 310-390 nm, the assumption is valid at least for this λ_x range. For λ_x = 310-390 nm, calculations were made versus both standards and the results were averaged. For λ_x = 410-490 nm, only Rubipy could be used as a standard. The integrals are approximated by numerical summation of $F_c(\lambda_x,\lambda_m)$ over the entire measured λ_m range.

Calculation of $\eta(\lambda_x,\lambda_m)$

To determine $\eta(\lambda_x,\lambda_m)$, each of the ten emission spectra for each sample is normalized so that the total area under each curve is equal to $\Phi_f(\lambda_x)$. $\eta(\lambda_x,\lambda_m)$ is then represented by the array of normalized emission spectra. This is done via the equation

$$\eta(\lambda_x,\lambda_m) = \phi_f(\lambda_x) \frac{F_c(\lambda_x,\lambda_m)}{\int F_c(\lambda_x,\lambda_m)\, d\lambda_m} \qquad (3)$$

where the integral is approximated in the same manner as it is for Eq. 2. Each point on the surface of $\eta(\lambda_x,\lambda_m)$ is equal to the quanta fluoresced per nm of λ_m per quanta absorbed at λ_x.

Results and Discussion

Mass-specific absorption spectra

Mass-specific absorption coefficients for FA and HA, $a^*_f(\lambda)$ and $a^*_h(\lambda)$ (m^2/g), are derived from absorbance measurements via the equation

$$a^*(\lambda) = \frac{2.303\ A(\lambda)}{C\ l} \qquad (4)$$

where $A(\lambda)$ = absorbance, C = concentration in mg/l, and l = pathlength in meters. Such spectra are typically exponential in shape with absorption increasing as

wavelength decreases (Zepp and Schlotzhauer, 1981; Carder et al., 1989). Thus, the spectra can be accurately described by the function

$$a^*(\lambda) = a^*(350) \exp[-S(\lambda-350)] \quad (5)$$

or by its logarithmic form

$$\ln[a^*(\lambda)] = \ln[a^*(350)] - S(\lambda-350) \quad (6)$$

where S (called the "spectral slope" parameter) is in nm^{-1} and λ is wavelength in nm. Thus, the absorption characteristics of each sample can be described by $a^*(350)$ and S, and the closeness of the fit (r^2) can be determined by regression on the linear equation. Figure 2 shows $a^*(\lambda)$ spectra for most of the samples with the ordinate scaled logarithmically, and the parameters of fit are listed in Table 2 along with some previously reported values. Some of the HA samples had masses too small to measure accurately, and their spectra are not displayed in Figure 2.

Comparing the values of $a^*(350)$ and S determined in this study to those of Carder et al. (1989), it is seen that these $a^*_f(350)$ are higher, $a^*_h(350)$ are close to, S_f are lower, and S_h are greater than or equal to the Carder et al. (1989) values. In the FA/HA fractionation process, pH was not measured but estimated, which can lead to FA samples that are contaminated by some HA or vice versa. The first case would lead to higher a^*_f and lower S_f values than would be expected if fractionation had been complete and the second case would lead to lower a^*_h and higher S_h values. Based on the comparisons above it seems more likely that, if anything, some of the FA samples are contaminated by HA. This can also explain in part the low HA yields.

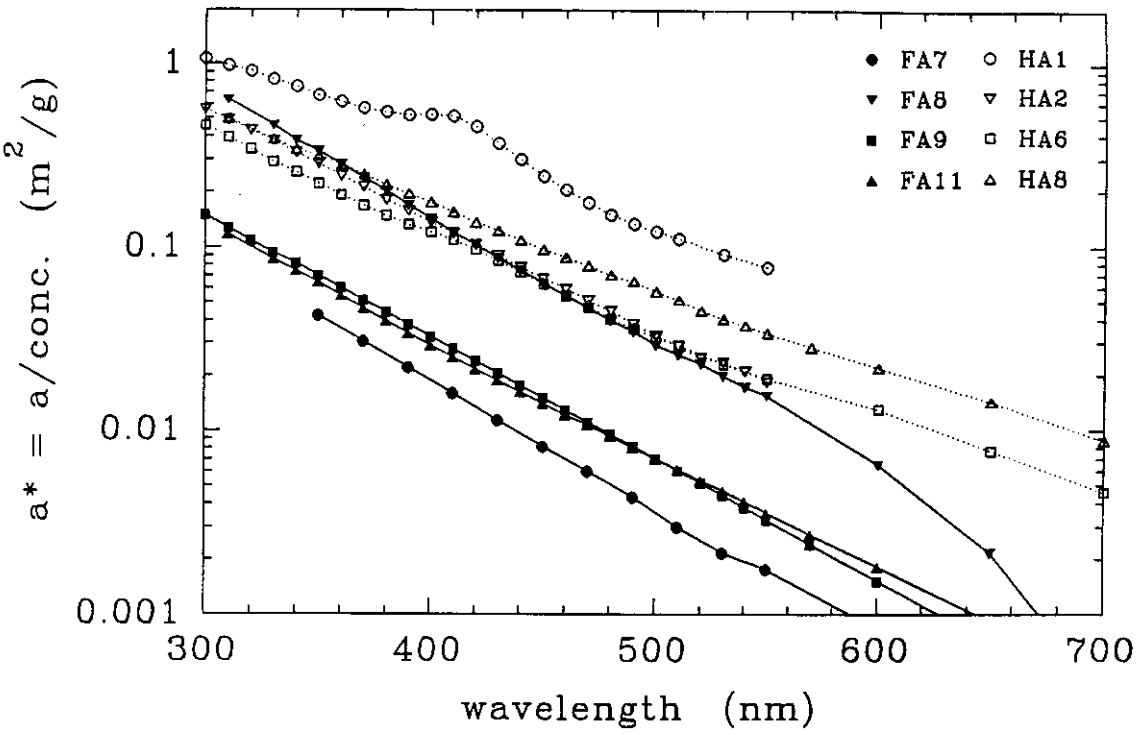

Figure 2. FA and HA specific absorption spectra, $a^*(\lambda)$. Note the linear nature of the curves when the ordinate is scaled logarithmically. FA is typically less absorbing than HA and the slope of the line is generally steeper. Some of the HA curves are not depicted because the isolated weights were too small to measure. The bump at 410 nm on the HA1 curve is possibly due to some pheophytin-like substance.

$\Phi_f(\lambda_x)$ measurements

Measured $\Phi_f(\lambda_x)$ vs. λ_x for the 4 FA samples are graphed in Figure 3a. FA has typical $\Phi_f(\lambda_x)$ values in the range of 0.010 to 0.015, with the exception of FA7 which fluoresces light absorbed in the 430-470 nm range quite strongly. There appears to be a local peak in fluorescence efficiency for most FA samples at λ_x = 370 nm. Similarly, Donard et al. (1987), by comparing absorption and fluorescence excitation spectra, found a broad maximum in fluorescence efficiency for Suwanee River FA at λ_x = 350-390 nm. $\Phi_f(\lambda_x)$ decreases at the high and low ends of the λ_x range for the FA samples, with the exception of the high wavelength end of FA9. This is due to the fact that FA9 has a sharp fluorescence emission peak at $\lambda_x/\lambda_m \approx$ 490/585 nm, possibly due to some phycoerythrin-like substance (Yentsch and Yentsch, 1979) incorporated into the FA structure. All the FA samples investigated have similar $\Phi_f(\lambda_x)$ values for $\lambda_x < 400$ nm, but the values diverge for $\lambda_x > 400$ nm.

Measured $\Phi_f(\lambda_x)$ vs. λ_x for the 7 HA samples are depicted in Figure 3b with a range of $\Phi_f(\lambda_x)$ values from 0.005 to 0.013. The HA samples show less variation in $\Phi_f(\lambda_x)$ as a function of λ_x than the FA samples, but there is still a slight peak at λ_x = 370 nm. $\Phi_f(\lambda_x)$ decreases as λ_x approaches 490 nm but there is no clear decrease as λ_x approaches 310 nm. Unlike FA, $\Phi_f(\lambda_x)$ values for HA vary considerably from sample to sample for $\lambda_x < 400$ nm. This can also be partially explained by inconsistent FA/HA fractionation i.e. since total mass yields of HA were small, its properties can be greatly affected by any contamination (with FA) or loss (of HA).

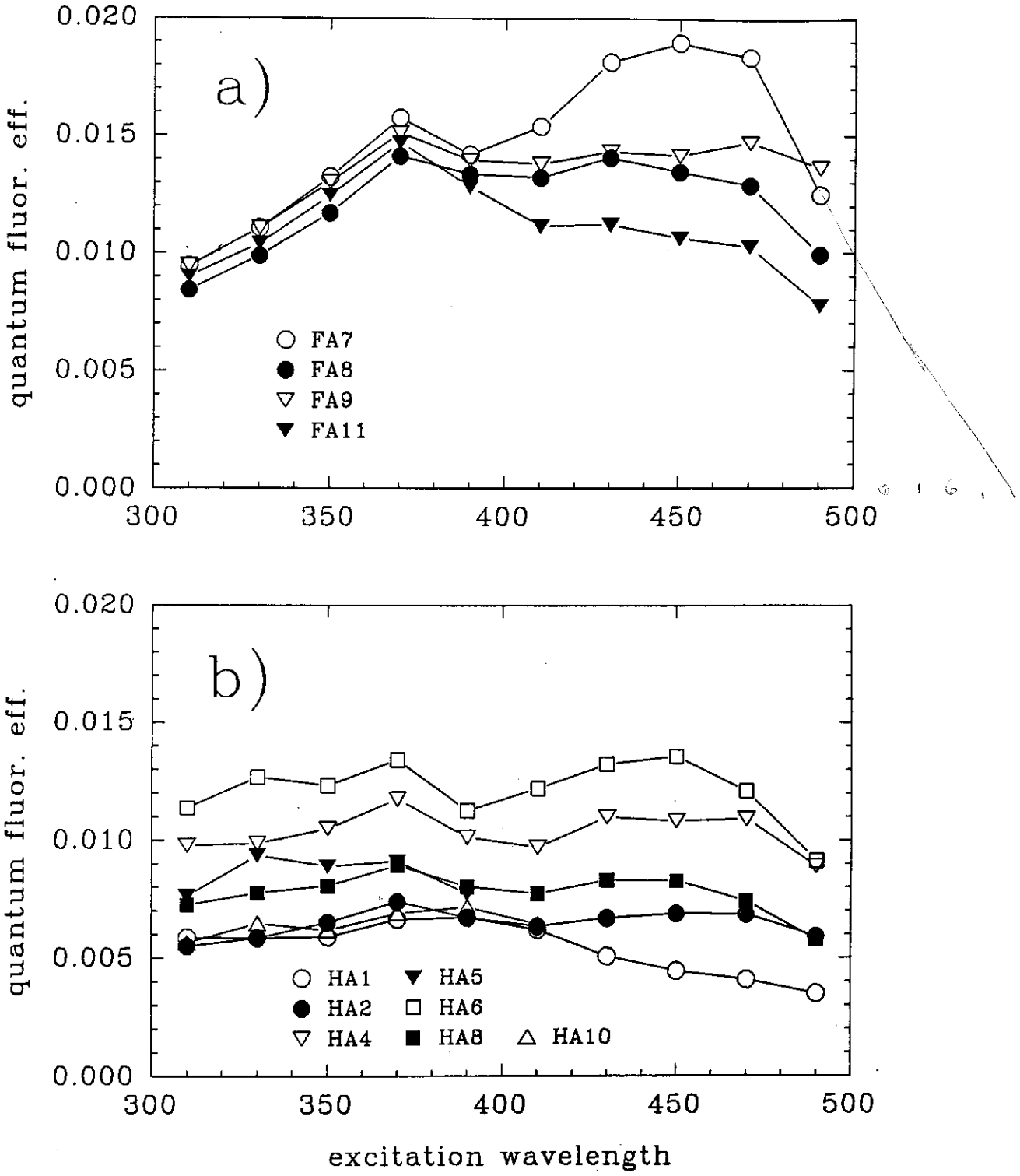

Figure 3. Quantum fluorescence efficiencies, $\Phi_f(\lambda_x)$ for a) FA and b) HA.

Trends in the a^* and Φ_f data

Some interesting relationships can be found by examining the a^* and Φ_f data in terms of the FA/HA fractions and the sources of origin. From Figure 2 and Table 2, it can be seen that a^* for HA is generally larger than that for FA, and that $a^*(350)$ for soils is greater than that for freshwater aquatic humus which is greater than that for marine humus. These trends are consistent with the observations that 1) low molecular weight humus usually absorbs less strongly per unit weight than high molecular weight humus (Ghassemi and Christman, 1968; Stewart and Wetzel, 1981; Hayase and Tsubota, 1985); 2) FA is typically of lower molecular weight than HA (Ghassemi and Christman, 1968; Stuermer, 1975; Hayase and Tsubota, 1985; Reid et al., 1990); and 3) marine humus has lower molecular weights than soil humus (Carder et al., 1989).

On the other hand, Φ_f for FA is generally greater than that for HA. Also, $\Phi_f(350)$ for marine CDOM averages about 0.010, while Zepp and Schlotzhauer (1981) found that $\Phi_f(350)$ was about 0.003 for freshwater aquatic humus and about 0.001 for soil humus. These trends are consistent with the observation that Φ_f is inversely related to molecular weight (Ghassemi and Christman, 1968; Stewart and Wetzel, 1980, 1981; Carlson and Shapiro, 1981; Visser, 1983) along with observations 2) and 3) above.

The two trends for a^* are the reverse of those for Φ_f. In other words, it appears that the more strongly a humus sample absorbs per unit mass, the less

efficiently it fluoresces. It has been hypothesized (Stuermer, 1975; Harvey et al., 1983) that HA forms from FA in the marine environment, making FA younger than HA. These observations lead to the following hypothesis: newly formed marine humus absorbs weakly but fluoresces strongly; as it ages, more chromophores are formed that absorb but do not fluoresce such that a^* increases and Φ_f decreases. Under this assumption, much of the variability in Φ_f could be due to variability in the abundance of absorbing chromophores, whereas fluorescing chromophores may act in a more or less conservative manner throughout the lifetime of the humus in the water column. However, this hypothesis is highly speculative and it represents one of many possible interpretations of the observations. For instance, the apparent inverse relationship between Φ_f and molecular weight can also be explained by the fact that a large molecule can provide more deactivation pathways for the excited state, or that it is more likely to quench its own fluorescence.

The hypothesis can be applied to the FA and HA data presented in this study. From Figure 2, it can be seen that a^* for FA isolated from different sites follows the trend [mouth of Tampa Bay] > [North Atlantic] > [mid-West Florida Shelf], and that a^* for HA follows the trend [Peruvian upwelling] > [mouth of Tampa Bay] > [mid-West Florida Shelf]. Trends for Φ_f for humus isolated from different sites are, for FA, [mid-West Florida Shelf] > [mouth of Tampa Bay] $\approx$ [North Atlantic], and for HA, [mid-West Florida Shelf] > [mouth of Tampa Bay] > [Peruvian upwelling]. Again, the trends for a^* are the reverse of those for Φ_f. Under the hypothesis proposed above, the humus from the mid-West Florida Shelf is likely of lower

molecular weight and of more recent origin than is the humus from the mouth of Tampa Bay. However, interpretation of the a^* and $\Phi_f(\lambda_x)$ data for these FA and HA samples is clouded by many other factors - low recoveries of humus, inconsistent FA/HA fractionation, complex mixtures of sources, and uncertain effects of photolysis. For instance, the high a^* values for the Peruvian upwelling site are probably due to a lower degree of photolysis, since the humus comes from depth.

Nonetheless, it would be a boon to DOM research if absorption and fluorescence measurements can be shown to provide insight into the nature of CDOM, since optical measurements can be made much more easily and rapidly than chemical ones. Further research should be carried out to validate the above hypothesis, keeping the following in mind: 1) recovery efficiencies should be as high as possible to ensure that the humus samples are representative of the water sample of origin, 2) consistent and exacting chemical isolation/fractionation procedures should be employed, 3) the effects of photolysis should be controlled, and 4) molecular weight fractionation should be investigated.

$\eta(\lambda_x,\lambda_m)$ measurements

Figures 4a-4k (top charts) show the measured $\eta(\lambda_x,\lambda_m)$ functions as surface plots for all FA and HA samples. All of the $\eta(\lambda_x,\lambda_m)$ surfaces have a dominant maximum at $\lambda_x/\lambda_m \approx 450/520$ nm except for those of samples HA5 and HA10 which have no data for $\lambda_x > 410$ nm. There is also usually a shoulder at $\lambda_x/\lambda_m \approx 370/480$

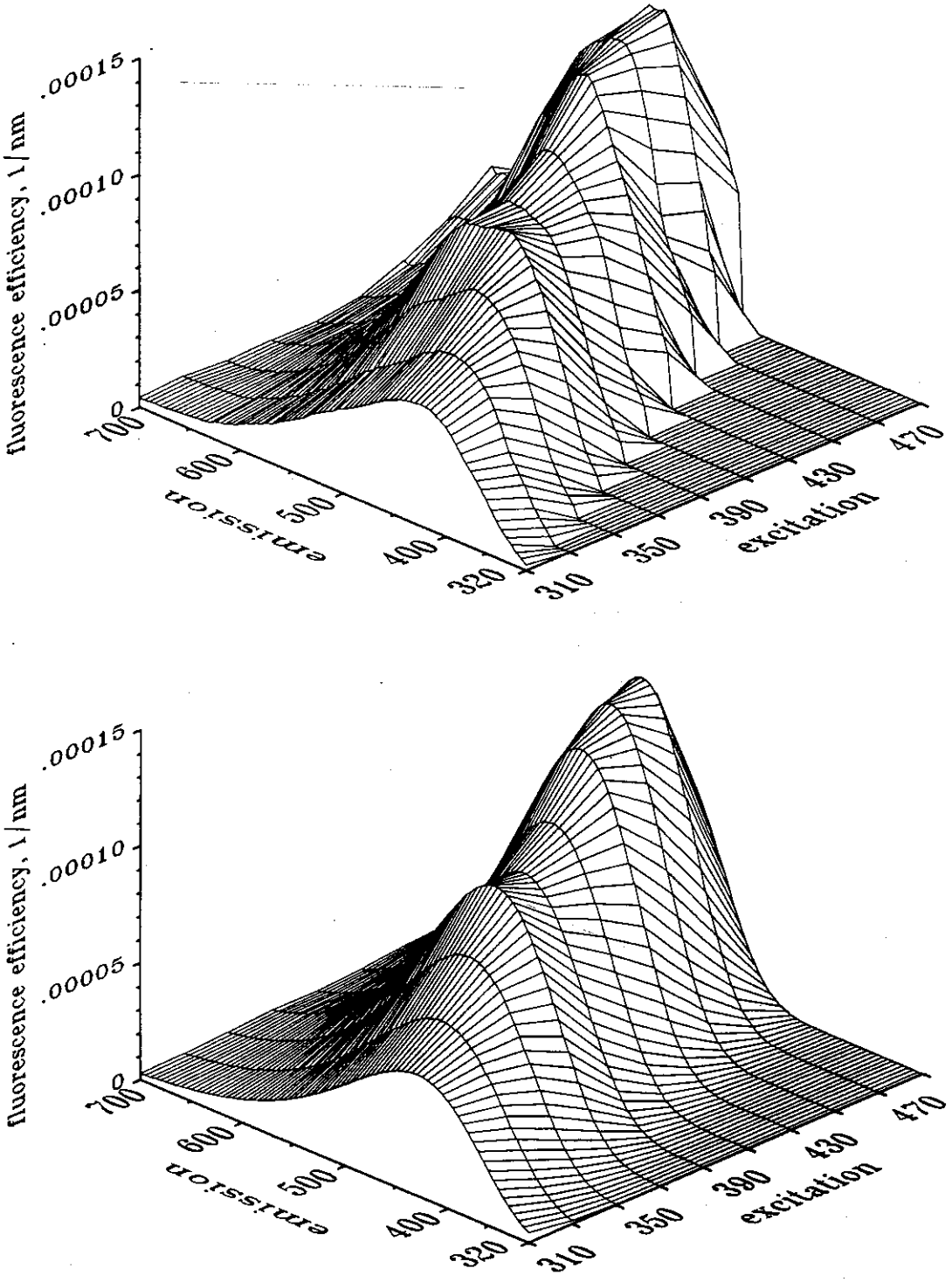

Figure 4a. Measured (top) and modeled (bottom) $\eta(\lambda_x,\lambda_m)$ surfaces for FA7. The ordinate represents quanta fluoresced in a 1 nm λ_m interval per quanta absorbed at λ_x.

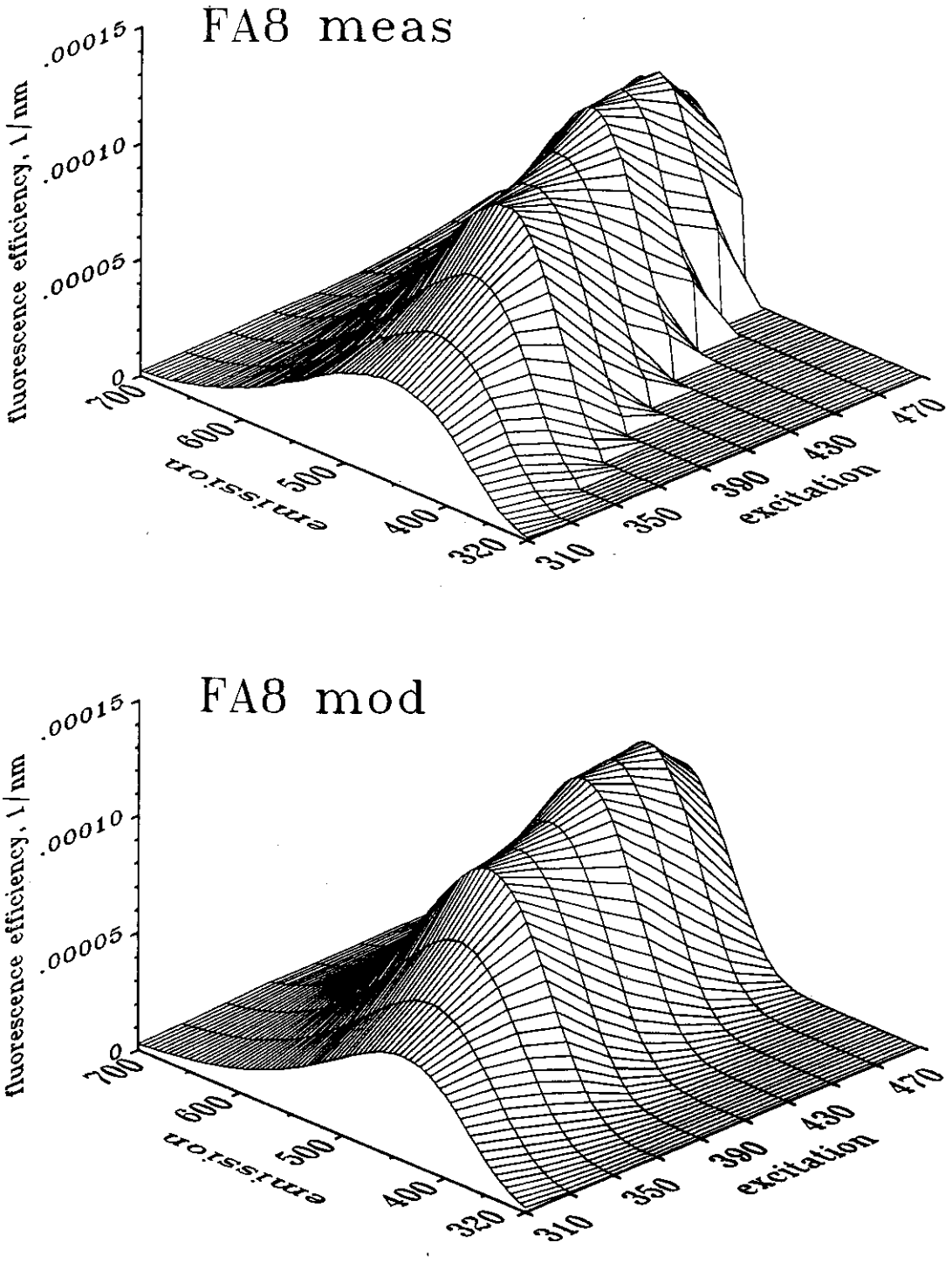

Figure 4b. Measured (top) and modeled (bottom) $\eta(\lambda_x,\lambda_m)$ surfaces for FA8. The ordinate represents quanta fluoresced in a 1 nm λ_m interval per quanta absorbed at λ_x.

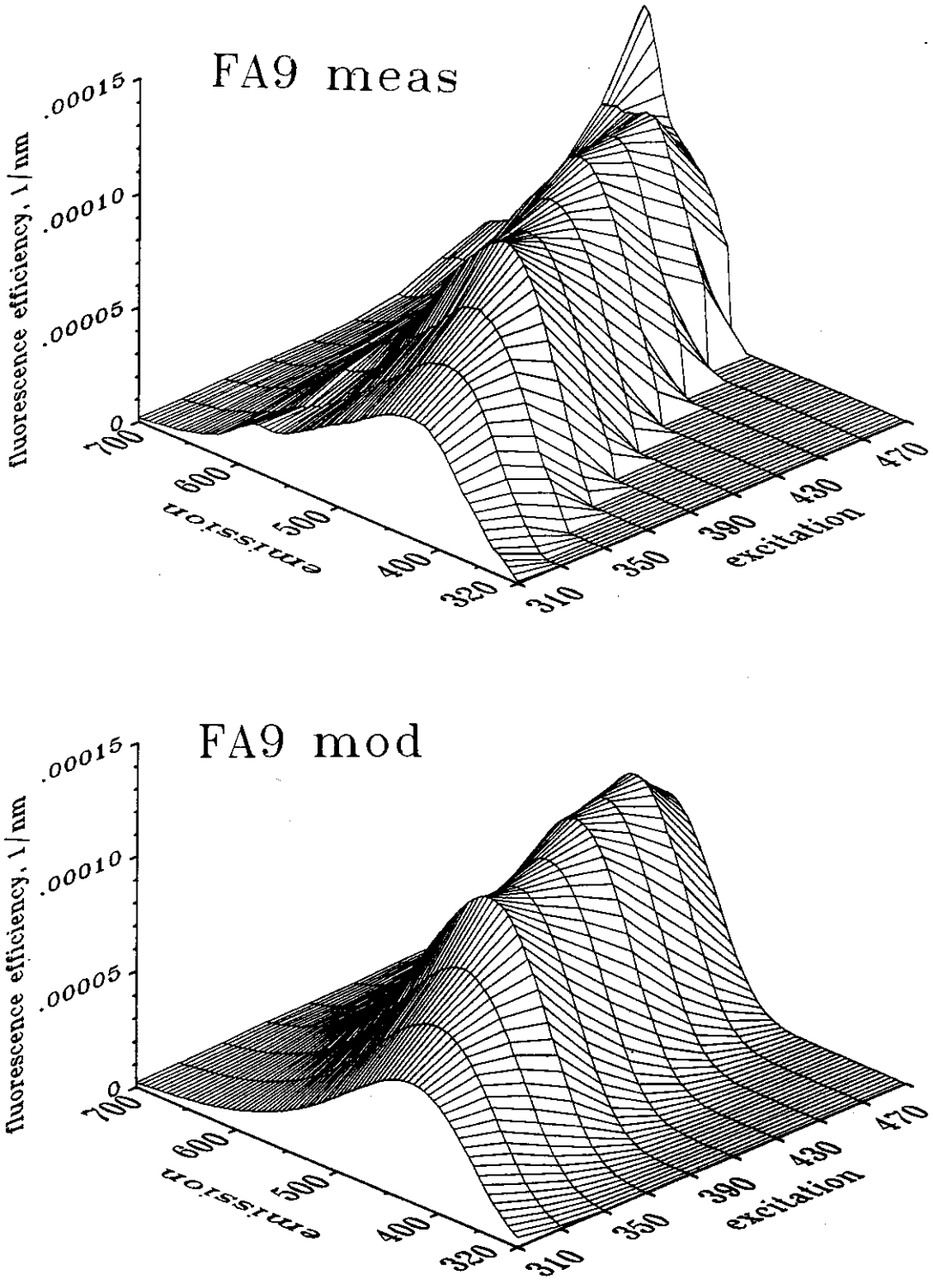

Figure 4c. Measured (top) and modeled (bottom) $\eta(\lambda_x,\lambda_m)$ surfaces for FA9. The ordinate represents quanta fluoresced in a 1 nm λ_m interval per quanta absorbed at λ_x.

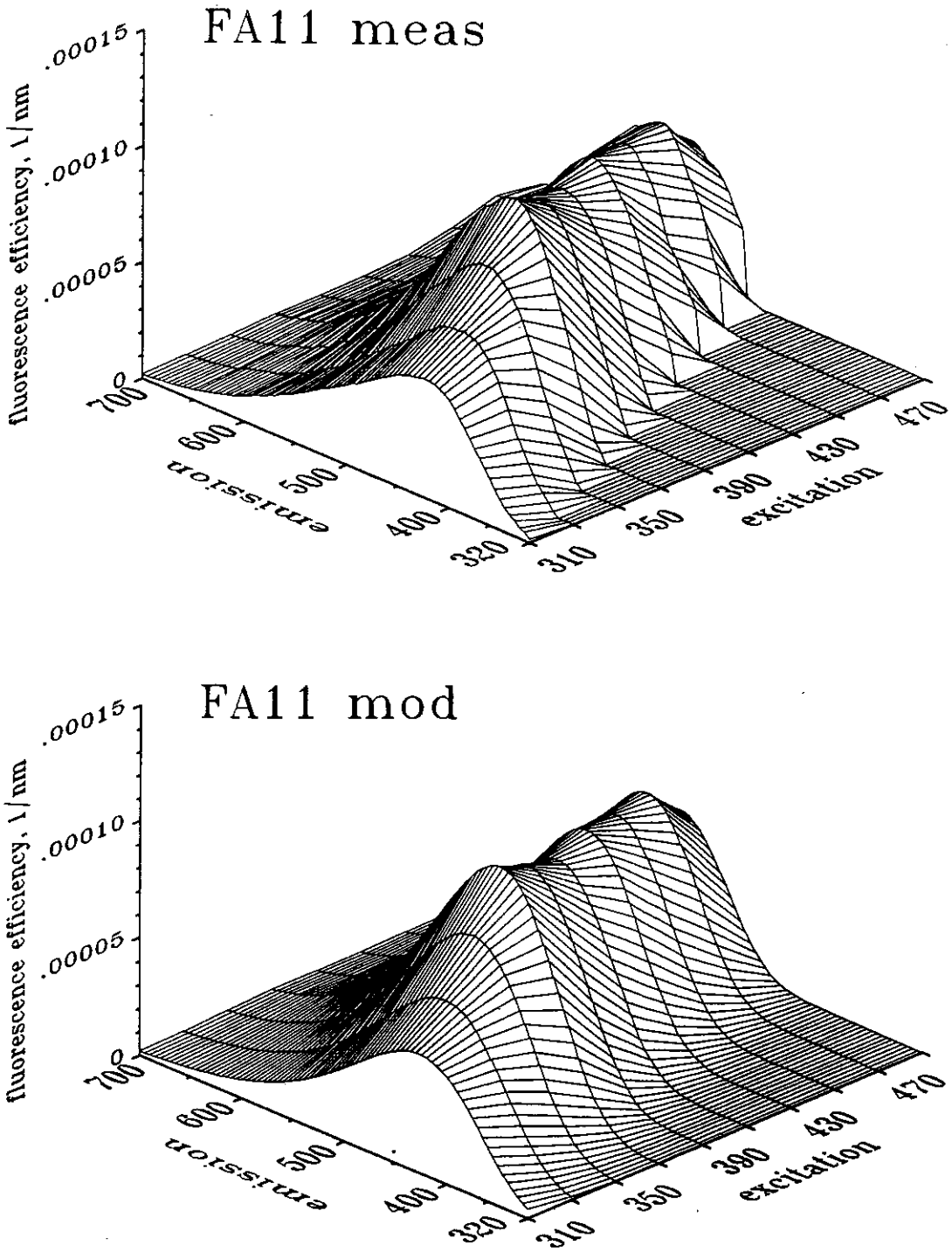

Figure 4d. Measured (top) and modeled (bottom) $\eta(\lambda_x,\lambda_m)$ surfaces for FA11. The ordinate represents quanta fluoresced in a 1 nm λ_m interval per quanta absorbed at λ_x.

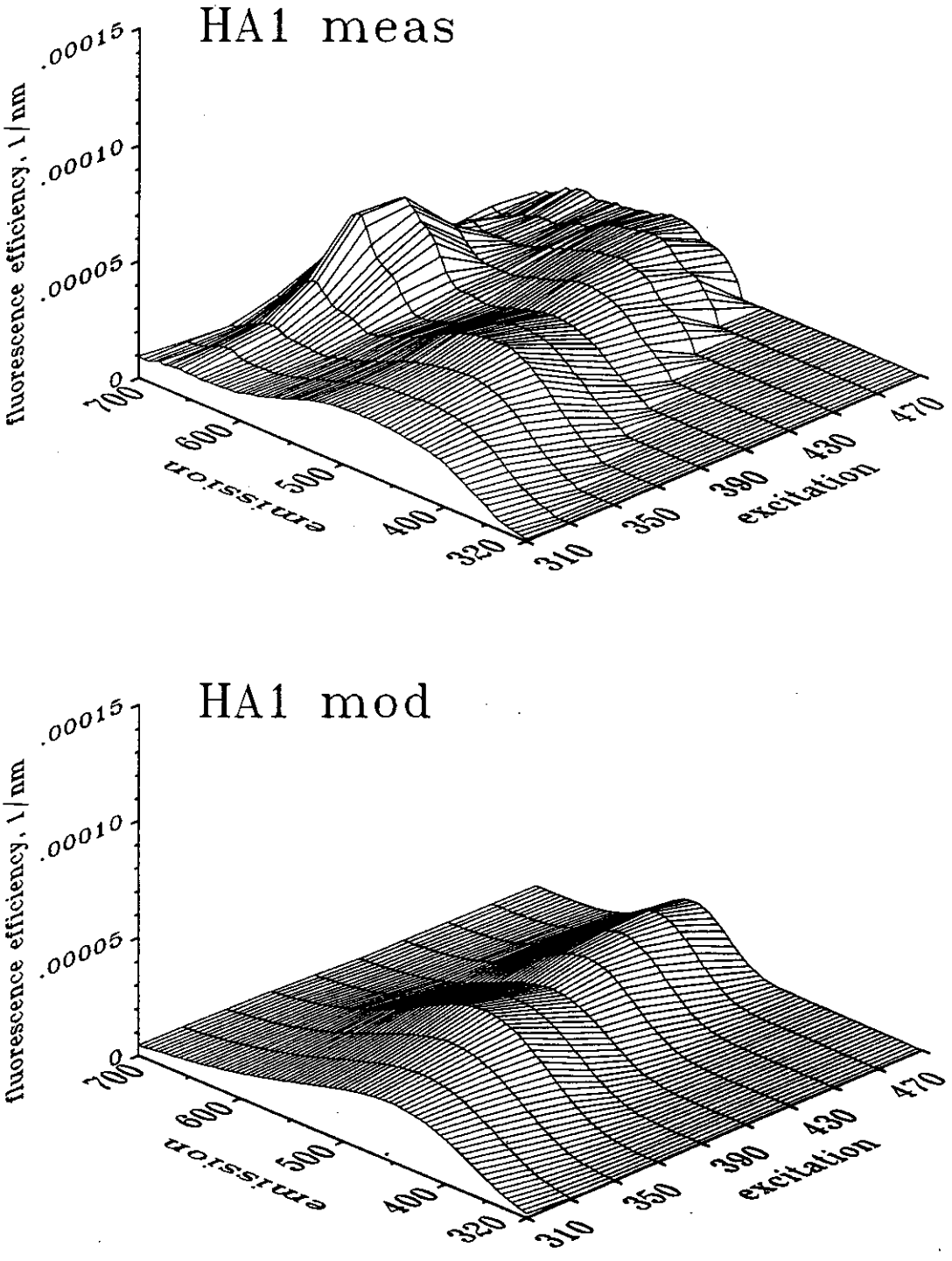

Figure 4e. Measured (top) and modeled (bottom) $\eta(\lambda_x,\lambda_m)$ surfaces for HA1. The ordinate represents quanta fluoresced in a 1 nm λ_m interval per quanta absorbed at λ_x.

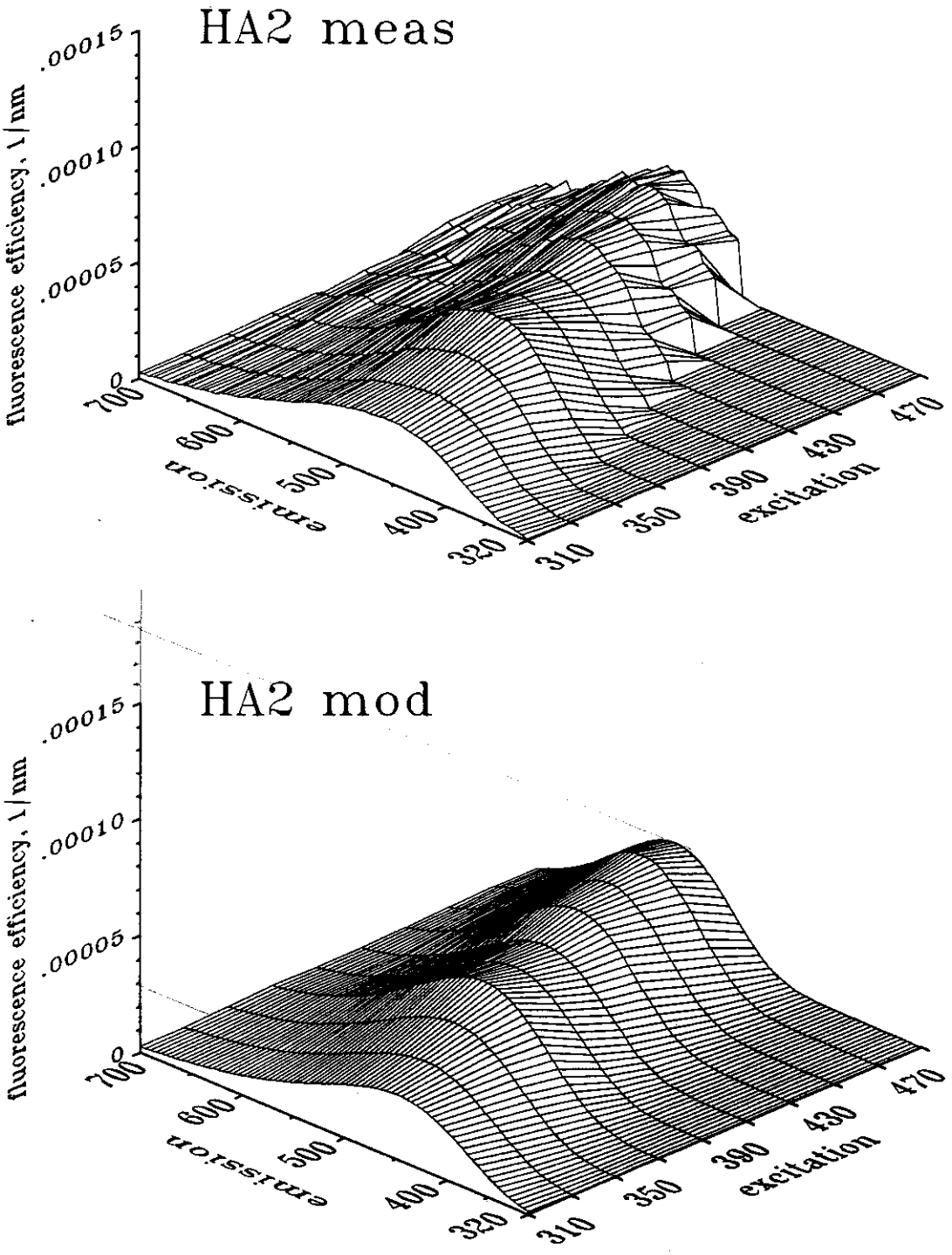

Figure 4f. Measured (top) and modeled (bottom) $\eta(\lambda_x,\lambda_m)$ surfaces for HA2. The ordinate represents quanta fluoresced in a 1 nm λ_m interval per quanta absorbed at λ_x.

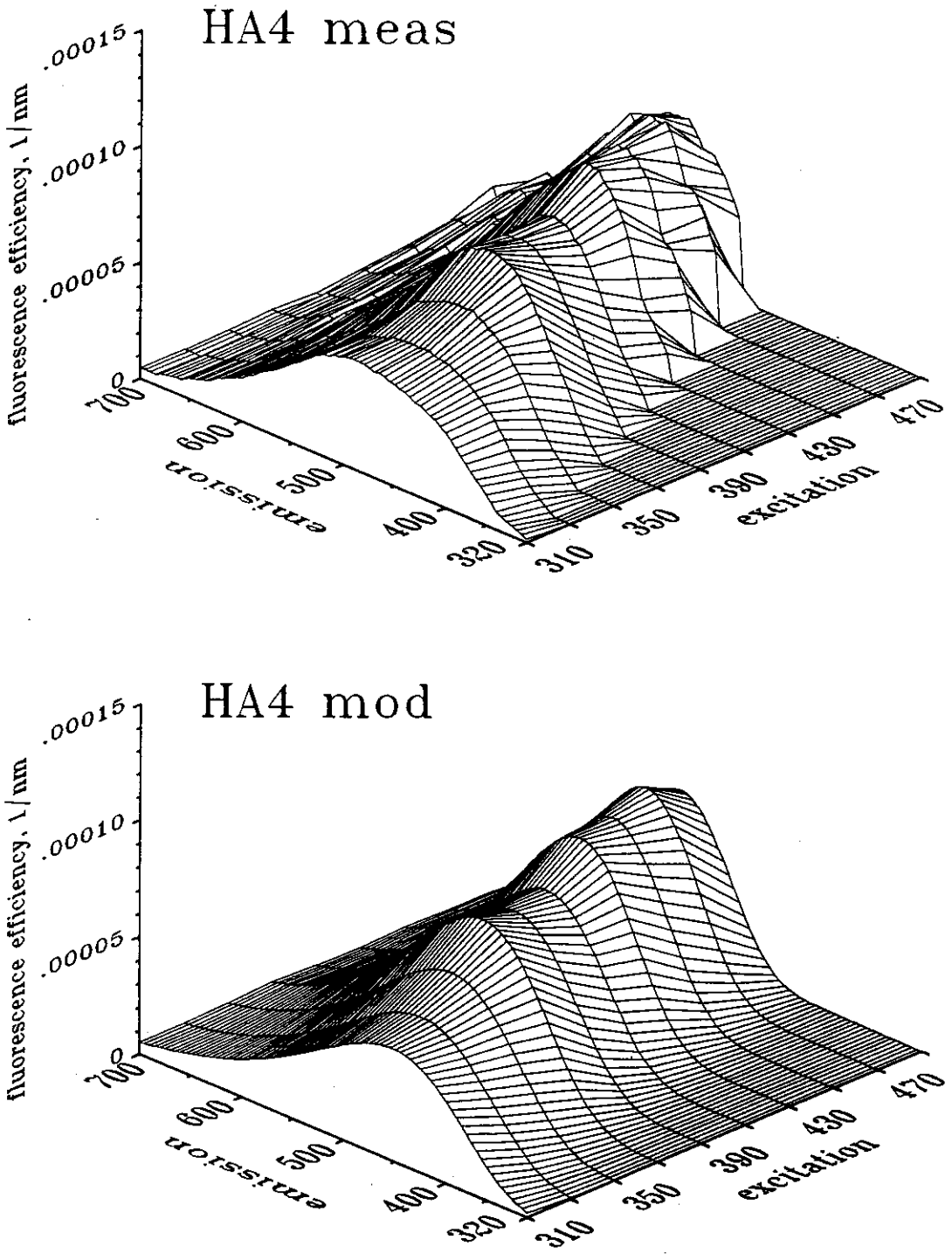

Figure 4g. Measured (top) and modeled (bottom) $\eta(\lambda_x,\lambda_m)$ surfaces for HA4. The ordinate represents quanta fluoresced in a 1 nm λ_m interval per quanta absorbed at λ_x.

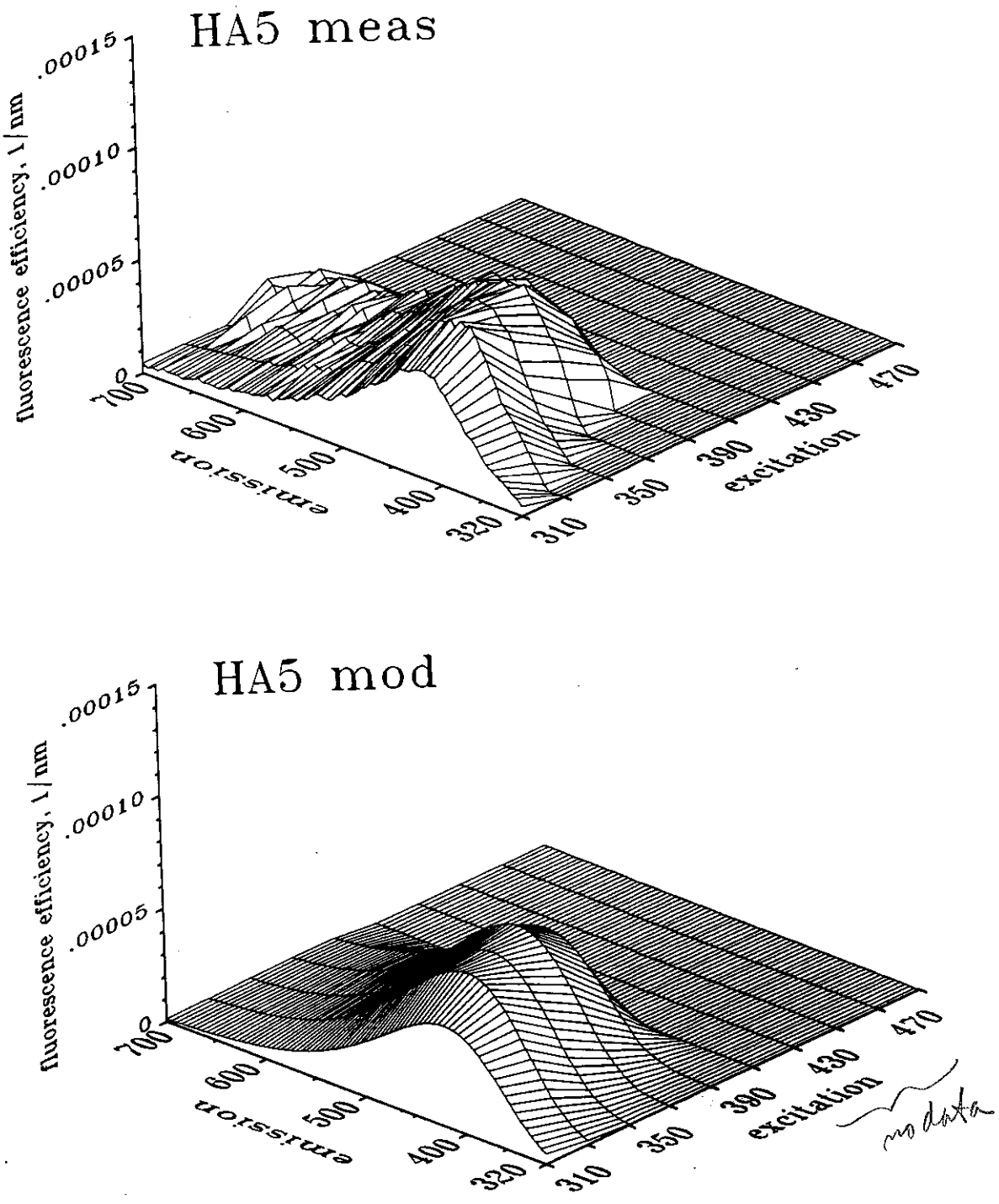

Figure 4h. Measured (top) and modeled (bottom) $\eta(\lambda_x,\lambda_m)$ surfaces for HA5. The ordinate represents quanta fluoresced in a 1 nm λ_m interval per quanta absorbed at λ_x.

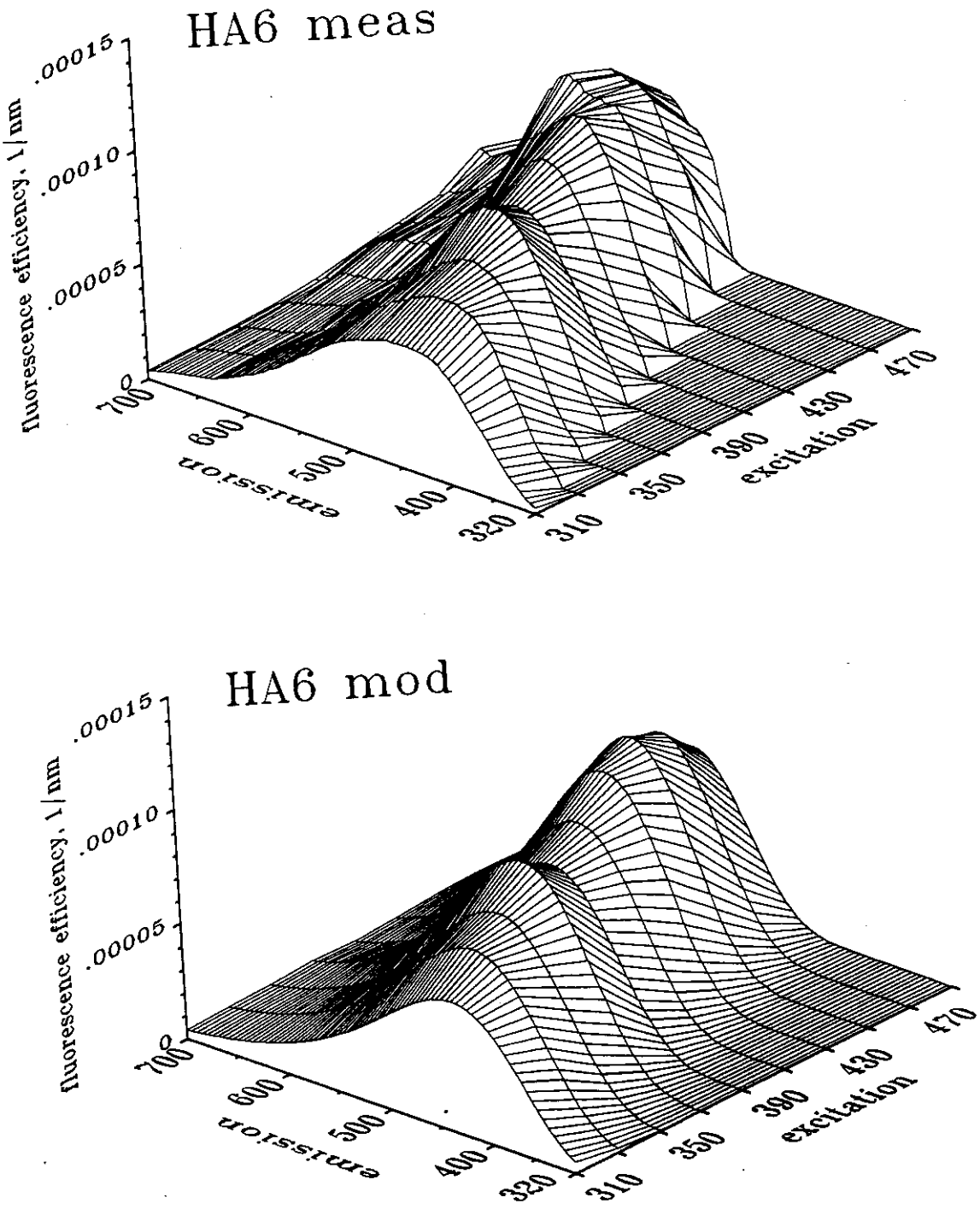

Figure 4i. Measured (top) and modeled (bottom) $\eta(\lambda_x,\lambda_m)$ surfaces for HA6. The ordinate represents quanta fluoresced in a 1 nm λ_m interval per quanta absorbed at λ_x.

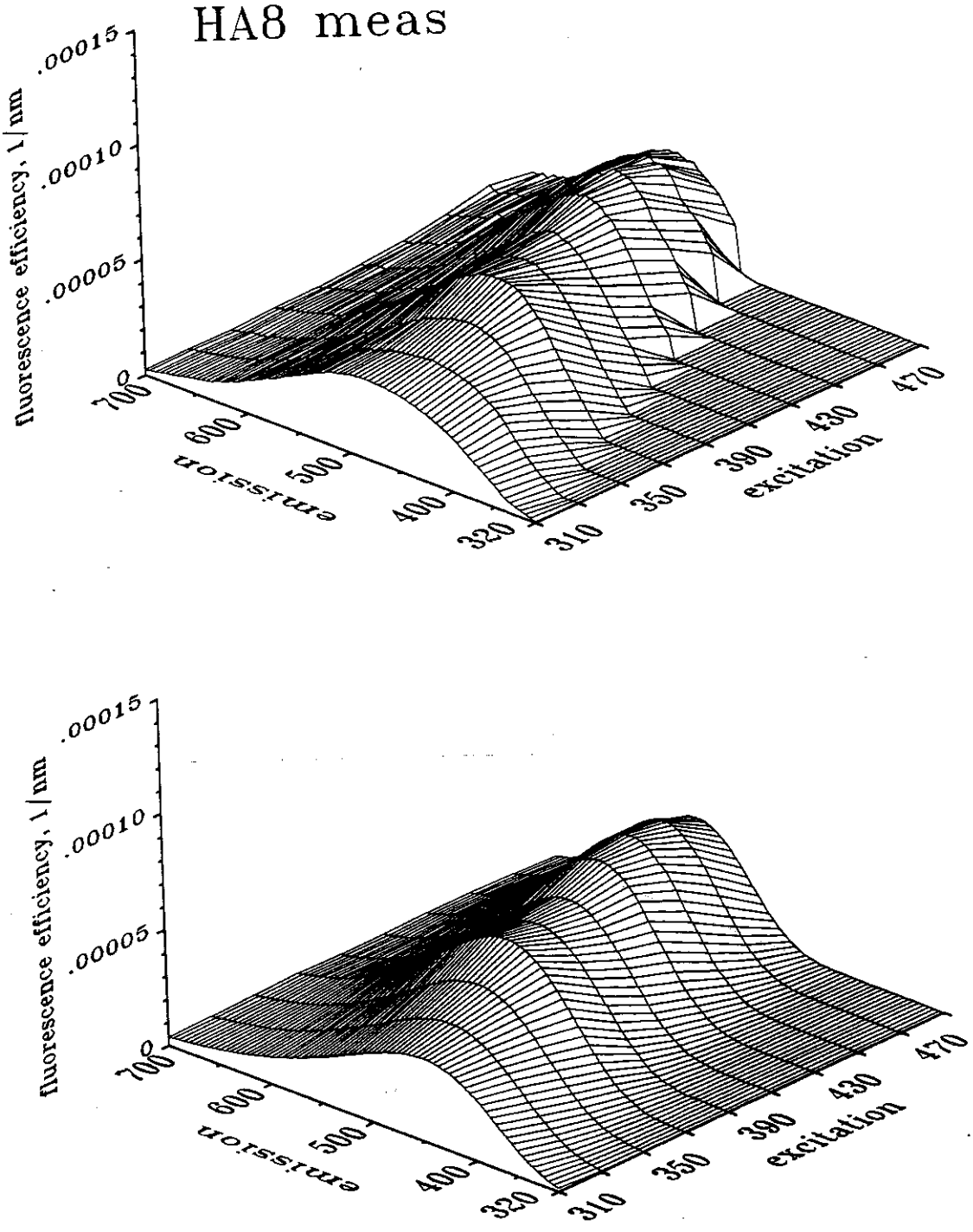

Figure 4j. Measured (top) and modeled (bottom) $\eta(\lambda_x,\lambda_m)$ surfaces for HA8. The ordinate represents quanta fluoresced in a 1 nm λ_m interval per quanta absorbed at λ_x.

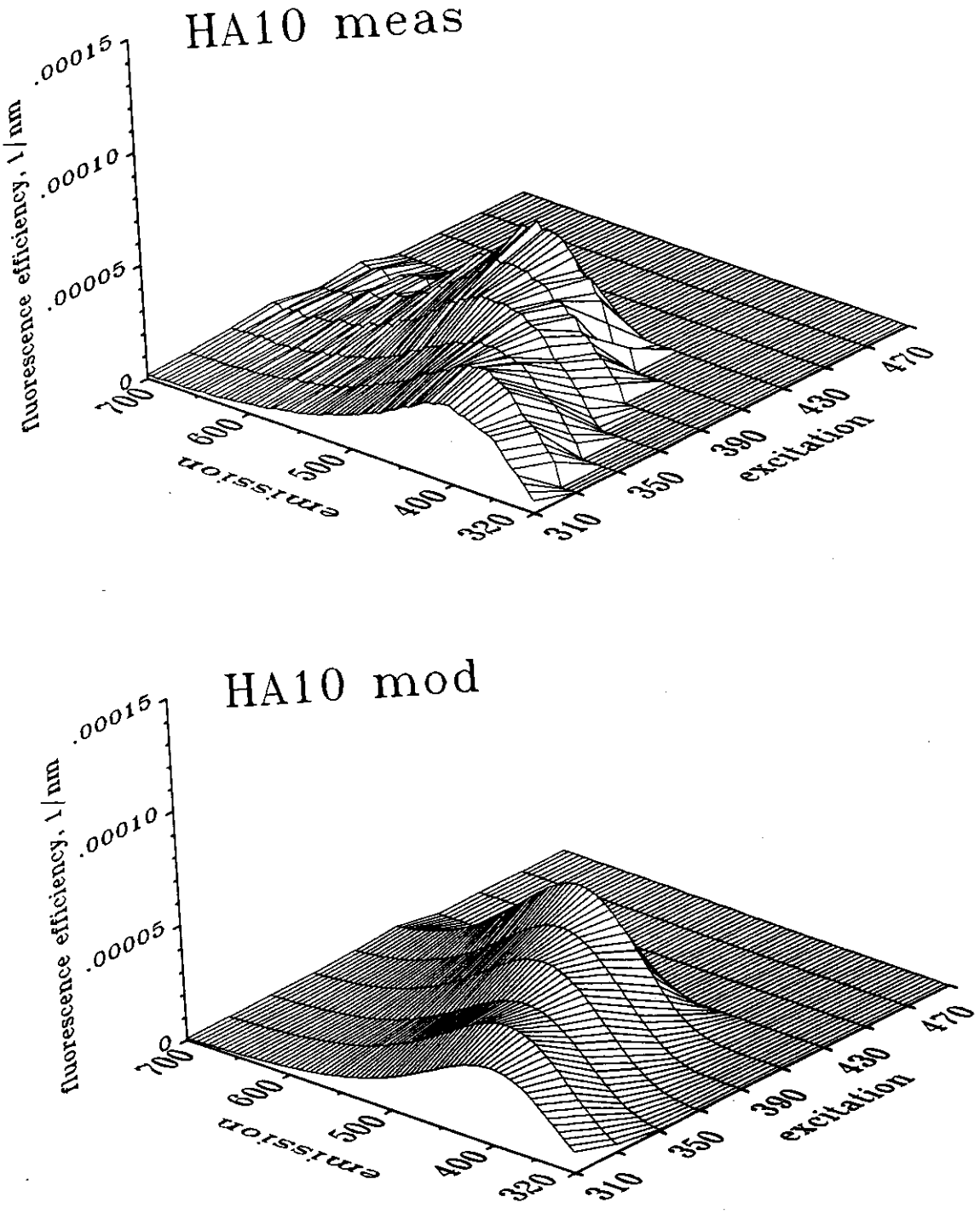

Figure 4k. Measured (top) and modeled (bottom) $\eta(\lambda_x,\lambda_m)$ surfaces for HA10. The ordinate represents quanta fluoresced in a 1 nm λ_m interval per quanta absorbed at λ_x.

nm corresponding to the local maximum in $\Phi_f(\lambda_x)$ at 370 nm found in most of the samples.

Two of the samples exhibited fluorescence peaks that suggest that other pigments were incorporated into their humic structures. Sample FA9, isolated from the North Atlantic, has a phycoerythrin-like peak at $\lambda_x/\lambda_m \approx 490/585$ nm (Yentsch and Yentsch, 1979), while HA1, isolated from the Peruvian Upwelling area, has a pheophytin-like peak at $\lambda_x/\lambda_m \approx 400/650$ nm (based on fluorescence work done in this lab). Furthermore, there is evidence in the literature that pigments can be incorporated into humic substances. For example, Ertel and Hedges (1983) found pheophytin absorption peaks in 4 different marine sedimentary HA samples, with stronger absorption bands in HA from reducing sediments, while Stuermer and Payne (1976) state that the incorporation of lipids and pigments into a marine FA sample could explain the results they obtained using ^{13}C- and ^{1}H-NMR and IR absorption to investigate its structure. It is possible that the fluorophores responsible for pigment fluorescence are present throughout the water column, but do not get extracted on XAD-2 or C_{18} resins unless condensation or some other pathway has led to its incorporation onto a humic molecule

Emission spectra of pure substances that have a single fluorophore have identical shapes and peak emission wavelengths for all λ_x. Unlike pure substances, the fluorescence emission peaks for FA and HA progress to longer wavelengths with increasing λ_x. This can be explained by one general fluorophore that is highly substituted and/or cross-linked, yielding slightly different electronic configurations for

every occurrence of that fluorophore throughout a single large FA or HA sample, or by the presence of multiple fluorophores (Donard et al., 1989; Coble, 1992). These two models can also explain the broadness of the FA and HA fluorescence peaks i.e. one broad peak can be composed of a multitude of smaller, overlapping peaks.

The $\eta(\lambda_x,\lambda_m)$ functions derived here differ from the fluorescence excitation-emission matrices (EEMs) published by Coble et al. (1990, 1992) and Coble (1992) in that the EEMs exhibit the presence of three distinct fluorophores at $\lambda_x/\lambda_m \approx$ 230/450, 275/310, and 345/450 nm. The first two EEM fluorophores occur at shorter λ_x than the shortest λ_x used in this study and were thus not detected. The third EEM fluorophore probably corresponds to the dominant maximum observed in the $\eta(\lambda_x,\lambda_m)$ functions, but it occurs at shorter λ_x and λ_m. One reason for this apparent discrepancy is that the $\eta(\lambda_x,\lambda_m)$ functions are fluorescence *efficiencies* which measure fluorescence intensity per quanta absorbed, whereas the EEMs are given in terms of counts per second which is a measure of relative fluorescence intensity without regard to the number of quanta absorbed. In other words, the $\eta(\lambda_x,\lambda_m)$ functions have been divided through by the quanta absorbed at λ_x whereas the EEMs have not. Dividing the EEMs through by the number of quanta absorbed at λ_x increases the heights of the emission spectra taken at long λ_x relative to those taken at shorter λ_x, shifting the λ_x peak to the red. Furthermore, inspection of the $\eta(\lambda_x,\lambda_m)$ plots reveals that the maximum fluorescence for λ_x = 350 nm usually occurs at $\lambda_m \approx$ 450 nm, so it appears that the $\eta(\lambda_x,\lambda_m)$ plots and the EEMs may be qualitatively similar. However, since different methods were used to correct the $\eta(\lambda_x,\lambda_m)$ functions and the EEMs for

instrumental configuration, such simple comparisons are still open to question.

$\eta(\lambda_x,\lambda_m)$ for the whole CDOM sample can be calculated by assuming that CDOM = FA + HA and using one of the following two equations, depending on which absorption parameters are available (the spectral dependencies have been left off for brevity). If absorption coefficients, a (m^{-1}), for FA and HA are known, then

$$\eta_{cdom} = \frac{a_f \eta_f + a_h \eta_h}{a_f + a_h} \tag{7}$$

where the subscripts 'f' and 'h' refer to FA and HA, and absorption coefficients are at λ_x. If specific absorption coefficients, a^* (m^2/mg), and the FA fraction of total humus, $f = C_f/(C_f + C_h)$, are known, then

$$\eta_{cdom} = \frac{f a_f^* \eta_f + (1-f) a_h^* \eta_h}{f a_f^* + (1-f) a_h^*} \tag{8}$$

Mathematical model for $\eta(\lambda_x,\lambda_m)$

To use these data in optical models, the 3-D spectra can be stored in a data file, or the curves can be modeled mathematically. It was found that transforming both wavelength axes to wavenumber ($\nu = 10^7/\lambda$, where ν is in cm^{-1} and λ is in nm) allowed easier modeling of η. First, each individual emission scan for each sample was fit to a Gaussian function of the form

$$\eta(\nu_x,\nu_m) = A_0(\nu_x) \exp\left[- \left(\frac{\nu_m - \nu_0(\nu_x)}{0.6\ \Delta\nu(\nu_x)} \right)^2 \right] \quad (9)$$

where ν_x = excitation wavenumber in cm^{-1}, ν_m = emission wavenumber in cm^{-1}, A_0 = maximum emission in nm^{-1}, ν_0 = wavenumber of maximum emission in cm^{-1}, and $\Delta\nu$ ≈ curve width at half maximum in cm^{-1}. Second, readily modeled trends were sought for the three Gaussian parameters A_0, ν_0, and $\Delta\nu$ as a function of ν_x. It was found that, for each sample, $A_0(\nu_x)$ didn't vary in any easily modeled way, but that ν_0 and $\Delta\nu$ both varied linearly with ν_x. The linear regression coefficients for these two relationships were determined and substituted into Eq. 9 and the axes were converted back to wavelength to yield the general equation

$$\eta(\lambda_x,\lambda_m) = A_0(\lambda_x) \exp\left[- \left(\frac{1/\lambda_m - A_1/\lambda_x - B_1}{0.6\ (A_2/\lambda_x + B_2)} \right)^2 \right] \quad (10)$$

λ_x and λ_m are in nm, A_1 and A_2 are dimensionless, and B_1 and B_2 are in nm^{-1}. The parameters $A_0(\lambda_x)$, A_1, B_1, A_2, and B_2 are listed in Table 3 for each sample. Correlation coefficients (r^2) for the modeled vs. measured surfaces were determined using PV-WAVE software (Precision Visuals, Inc.), and averaged 0.985 when HA1, which has a large pheophytin-like peak that was not modeled, was excluded. Figures 4a-4k show comparisons of the measured (top) and modeled (bottom) $\eta(\lambda_x,\lambda_m)$ surfaces.

Table 3. Parameters for $\eta(\lambda_x,\lambda_m)$ model for FA and HA. A_0 is in units of nm^{-1}, A_1 and A_2 are dimensionless, and B_1 and B_2 are in nm^{-1}. A short dash (-) indicates that no data is available.

	FA7	FA8	FA9	FA11	HA1	HA2
$A_0(\lambda_x) \times 10^5$						
$\lambda_x = 310$	5.18	4.48	5.21	5.09	2.49	2.78
330	6.34	5.67	6.57	6.27	2.68	3.13
350	8.00	7.23	7.93	7.93	2.95	3.73
370	9.89	9.26	9.93	9.76	3.34	4.42
390	9.39	9.06	9.93	8.72	2.77	4.03
410	10.48	9.22	9.47	7.93	2.26	3.91
430	12.59	10.14	10.21	8.15	2.63	4.41
450	13.48	9.90	10.08	7.75	2.72	4.52
470	13.61	9.70	10.11	7.70	2.65	4.75
490	9.27	7.90	8.34	5.98	2.20	4.29
A_1	0.470	0.389	0.466	0.471	0.304	0.379
$B_1 \times 10^4$	8.077	10.073	8.340	8.204	12.169	10.043
A_2	0.407	0.386	0.386	0.386	0.591	0.362
$B_2 \times 10^4$	-4.57	-4.20	-4.13	-4.20	-9.39	-3.17
r^2	0.987	0.989	0.975	0.991	0.712	0.985

	HA4	HA5	HA6	HA8	HA10
$A_0(\lambda_x) \times 10^5$					
$\lambda_x = 310$	4.83	4.49	5.77	3.61	3.40
330	5.11	5.71	6.86	4.01	4.02
350	5.94	5.49	7.27	4.46	3.71
370	7.20	5.52	8.37	5.48	4.28
390	6.53	4.31	7.08	5.06	4.49
410	6.41	-	7.80	5.05	5.07
430	7.66	-	8.90	5.66	-
450	7.55	-	9.30	5.70	-
470	7.88	-	8.41	5.32	-
490	6.81	-	6.68	4.42	-
A_1	0.346	0.481	0.447	0.356	0.710
$B_1 \times 10^4$	10.891	8.314	8.594	10.694	2.161
A_2	0.411	0.311	0.417	0.406	0.490
$B_2 \times 10^4$	-4.60	-1.80	-4.64	-4.42	-6.65
r^2	0.985	0.985	0.985	0.986	0.987

Validity of using extracted samples

The assumption that the optical properties of CDOM can be approximated by summing the properties of extracted FA and HA can lead to errors if 1) the sample is altered in the isolation process or if 2) the recovery of CDOM from the water sample is incomplete and the optical properties of the unrecovered CDOM fraction differ from those of the recovered fraction.

Sample alteration. Sample alteration can be caused by contact with solvents such as MeOH and NH_4OH, reactions with the sorbent, resin bleed products in the final sample, or extreme pH. For instance, Stuermer (1975) found that small amounts of nitrogen were incorporated into humus samples that were eluted from XAD-2 using an NH_4OH eluant, and amine groups such as $-NH_2$, -NHR, and $-NR_2$ are known to increase the fluorescence intensity of aromatic centers while -NO and $-NO_2$ groups are known to decrease it (Visser, 1983). However, since marine humus has a low aromatic content (Harvey et al., 1983; Hedges et al., 1992), this should not be a problem. XAD-2 can continue to bleed small amounts of resin even after exhaustive cleaning procedures, and it is not known whether the bleed products from the styrene-divinylbenzeve structure will remain in the sample after freeze-drying. On the other hand, any resin bleed from C_{18} is expected to evaporate during freeze-drying (Nigel Simpson, Varian technical representative, personal communication). Amador et al. (1991) found that A(280), relative fluorescence intensity at λ_x/λ_m = 350/450

(F(365,490)), and H_2O_2 production capacity for water samples from both Biscayne Bay and the Sargasso Sea returned to 90-101% of their original values when they were passed thru C_{18} cartridges and then reconstituted with the extracts, indicating that contact with C_{18} does not affect the optical properties greatly. However, they also found that acidification of seawater to a pH of 2.3-2.5 followed by readjustment to the original pH tends to lower the absorbance and fluorescence. Thus, the pH changes encountered during the isolation process may lower the absorption and fluorescence of the extracted samples, but other possible alteration mechanisms appear to be limited.

CDOM recovery efficiency. The efficiency with which CDOM is recovered from the water sample depends on losses during extraction from seawater, elution from the sorbent, and in sample processing up to the final freeze drying. Recovery efficiency, REC, based on $a_{cdom}(350)$ has been calculated for several extracted water samples via the equation

$$REC = \frac{a_f^*(350)\ m_f + a_h^*(350)\ m_h}{a_{cdom}\ v} \qquad (11)$$

where m = total mass recovered in mg, v = volume of seawater processed in liters, and the subscripts 'f' and 'h' refer to FA and HA, respectively. The results, shown in Table 4, indicate REC values ranging from 2.5-22%. However, these values are probably lower than the actual recoveries because many of the reconstituted samples had noticable particles, indicating that dissolution was incomplete, which will lead to

Table 4. FA and HA recovery efficiency information. Trailing numbers on sample names correspond to a given extracted sample i.e. FA4 and HA4 are extracted from the same water sample. FA10 and FA11 are sub-fractions of the same sample. Total masses of HA recovered from samples 7, 9, 10, and 11 were too small to measure. Some FA samples here are not listed in Table 1. Recovery efficiency (REC) is calculated via Eq. 11.

sample name	volume (liters)	tot.mass (mg)	a*(350) (m^2/g)	a(350) (m^{-1})	REC
FA4	26	7.048	0.2025	2.347	0.026
HA4		0.156	0.913		
FA6	55	12.349	0.166	0.267	0.149
HA6		0.65	0.220		
FA7	32	12.66	0.0415	0.267	0.061
FA8	20	2.24	0.3312	1.115	0.039
HA8		0.42	0.3114		
FA9	55	19.06	0.0727	0.113	0.223
FA10	55	17.62	0.1463	0.301	0.183
FA11		6.99	0.0650		

to low a^* and REC values. The problem of incomplete dissolution is particularly acute because HA is difficult to dissolve and its high a^* values provide a large effect on REC.

An experiment was performed to determine the extraction efficiency of the XAD-2 method. A water sample taken from the pier at Fort De Soto Park (within Tampa Bay near the mouth) was acidified to pH 2 and passed over a 1.5 cm x 22 cm column of XAD-2. A(350) and F(350,450) were measured on aliquots sampled just upstream (A_u and F_u, respectively) and just downstream (A_d and F_d) of the column at several time intervals. The results are graphed in Figure 5 as A_d/A_u and F_d/F_u vs. time. Over the first several hours, extraction efficiencies were about 60% based on A(350), and 50% based on F(350,450), although this efficiency is likely to fall off as the sorbent gets loaded with humus, a trend which is noticable in Figure 5. The values above are low compared to those of Mantoura and Riley (1975), who extracted 82-87% of the CDOM based on A(250) from river and lake water using a 0.8 cm x 10 cm XAD-2 column. The lower efficiencies obtained in this experiment could be due to column geometry, high flow rate, different hydrophobic character of the CDOM from Tampa Bay - which has a significant amount of marine influence - versus that of the freshwater humics, or different extraction efficiencies for chromophores that absorb at 250 nm versus those that absorb at 350 nm by XAD-2.

Extraction efficiency for the C_{18} method was not measured, but Amador et al. (1991) determined values of 38-81% based on A(280) and 62-91% based on F(365,490) for a variety of waters using the 10 g C_{18} cartridges. They also found that

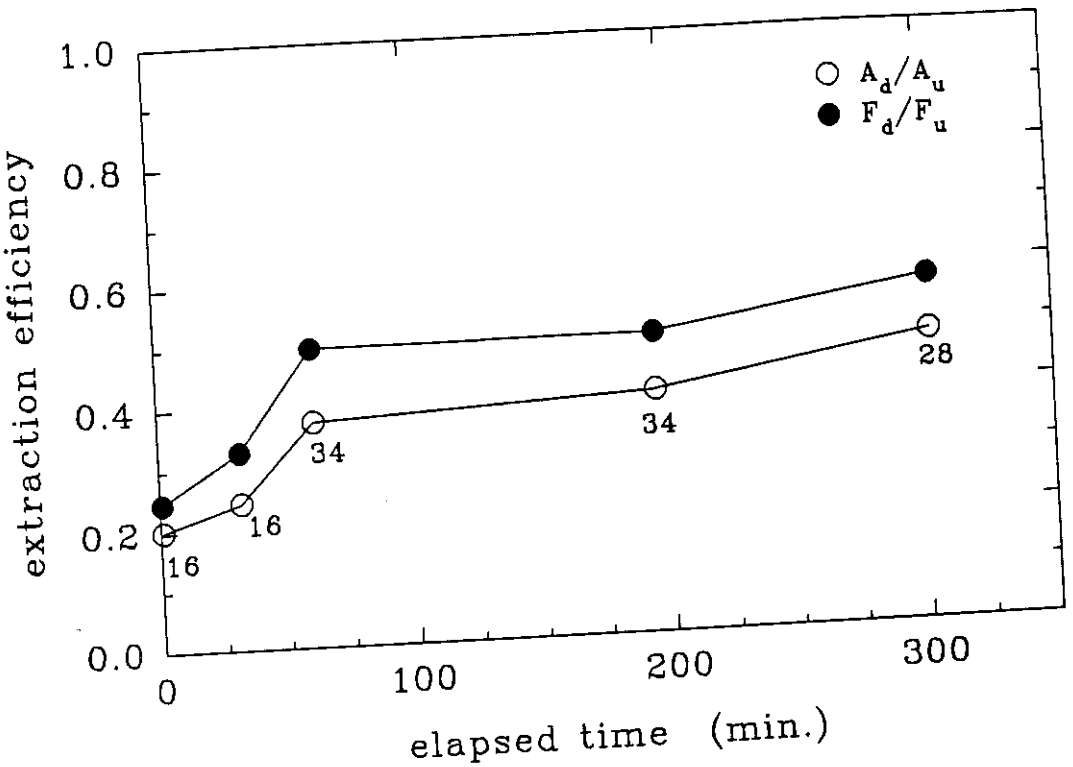

Figure 5. Extraction efficiency as a function of time for a water sample taken off Fort de Soto passed over a column of XAD-2 resin. A_d/A_u is the ratio of A(350) of an aliquot of the water sampled just downstream (subscript 'd') and just upstream (subscript 'u') of the column. F_d/F_u is the analogous ratio for F(350,450). The numbers below the symbols indicate the flowrate in ml/minute.

C_{18} extracted 1.8 and 1.2 times as much CDOM from Biscayne Bay water based on A(280) and F(365,490), respectively, than XAD-2, although very small amounts of both sorbents were used in this experiment. It seems reasonable to assume that both methods extract about half of the CDOM based on A(350), and that the low recovery efficiencies presented in Table 4 are due in part to actual losses during the remaining processing and in part to inaccurate a^* measurments due to incomplete dissolution of sample during reconstitution. Both the XAD-2 columns and the C_{18} cartridges used to isolate the samples usually retained a visible yellowish tinge after elution, indicating that some loss of sample definitely occurs during this step. This fraction is probably composed of HA-like, high molecular weight compounds. Supporting evidence for this statement are that 1) HA is generally less soluble than FA, 2) C_{18} is known to provide difficulties in eluting high molecular weight compounds (Nigel Simpson, personal communication), and 3) in most cases little or no HA was recovered from C_{18}-extracted samples. Another possible explanation for the low recoveries of HA for C_{18}-extracted samples is that some HA may have precipitated quickly after the initial acidification and been retained on the 0.2 uM filter. It is also possible that some CDOM is lost in the discarded CH_2Cl_2 from the lipid extraction step and in the 'white floc' that occasionally forms after elution from C_{18} cartridges (see Appendix 1). In any case, selective exclusion of HA and high molecular weight humus from the final isolates can help to explain the low REC values because their mass-specific absorption coefficients are generally quite high and REC is based on absorption.

Other considerations. Even if isolation procedures do not recover all of the CDOM, the fluorescence efficiency measurements may still be valid if it can be shown that the optical properties of the recovered fraction approximates that of the whole sample. $\Phi_f(355)$ measured on whole samples taken at two sites just west of Egmont Key during a cruise in May 1992 gave values of 0.0113 and 0.0089, while $\Phi_f(350)$ calculated from a*(350) and $\Phi_f(350)$ measured on the FA and HA samples extracted from the Egmont Key site during March 1990 yields a value of 0.0112. Due to the differences in time, these data do not directly demonstrate that the recovered fraction is representative of the whole sample, but they suggest that the $\Phi_f(\lambda_x)$ values are probably in the correct general range.

It may be possible to recover more humic material using XAD-8, an acrylic-ester resin (Thurman and Malcolm, 1981; Aiken, 1987, 1988). It absorbs water better than XAD-2, allowing faster sorption of the dissolved humic substances. It elutes more easily than XAD-2 in terms of *mass* (up to 95% elution efficiency), especially for high-molecular-weight compounds, but it remains to be seen if XAD-8 methodologies can recover more marine CDOM in terms of *optical properties*. It suffers from more resin bleed than XAD-2, but most of the product is methyl acrylic acid which evaporates when freeze-dried.

To avoid problems associated with the extraction procedure - incomplete recovery of CDOM from the seawater, contamination by resins and reagents, sample alteration, large amounts of seawater needed, etc. - future analyses could use whole samples which are unaltered except for filtration of particles (e.g. see Coble, 1992).

This approach should include measurement of dissolved organic carbon (DOC) on an aliquot of the sample in order to provide the link between optics and geochemical carbon cycles, although it is still unclear which methodology, wet UV-oxidation or platinum catalysis, yields more accurate results (Williams and Druffel, 1988). Although this method sacrifices the information gained from analysis of separate FA and HA fractions, the overall fluorescence efficiencies can still be used in many optical applications. A difficulty with this approach is that more sensitivity is required to accurately measure $a_{cdom}(\lambda)$ at visible wavelengths where the low CDOM absorption coefficients are confounded by absorption from water and particles.

PART 1 SUMMARY

1. $\Phi_f(\lambda_x)$ for FA and HA isolated from various oceanic waters ranged from 0.9 to 1.8% for FA and from 0.4 to 1.3% for HA. $\Phi_f(\lambda_x)$ typically has a local peak around λ_x = 370 nm, and seems to decrease as λ_x decreases towards 310 nm and increases towards 490 nm.

2. The a^* and Φ_f data presented here are consistent with the hypothesis that newly formed marine humus absorbs weakly but fluoresces strongly, and that much of the variability in Φ_f is due to variability in the abundance of absorbing chromophores, with fluorescing chromophores behaving more or less conservatively throughout the lifetime of the humus.

3. The values of $\eta(\lambda_x,\lambda_m)$ for CDOM can be calculated by combining the FA and HA $\eta(\lambda_x,\lambda_m)$ measurements, which can be reconstructed by applying the parameters in Table 3 to Eq. 8. The shapes of the individual emission curves for a given λ_x are very close to Gaussian when the fluorescence is plotted versus wavenumber rather than wavelength.

4. The $\eta(\lambda_x,\lambda_m)$ data presented are to my knowledge the first quantitative measures of

CDOM fluorescence efficiency as a function of both λ_x and λ_m. Such data are essential when modeling the effect of CDOM fluorescence on other oceanic optical properties (e.g. irradiance reflectance, water-leaving radiance, absorption meter measurements), and they also may prove to be useful for quantifying concentrations of CDOM itself. Since CDOM is ubiquitous in natural waters, $\eta(\lambda_x,\lambda_m)$ is likely to be an important portion of the inelastic scattering coefficient, which, along with the absorption and volume scattering coefficients, is an inherent optical property of natural waters.

PART 2: APPLICATIONS

In this section, the $\eta(\lambda_x,\lambda_m)$ measurements described in Part 1 are applied to 3 oceanographic problems. First, the effect of CDOM fluorescence on ocean color remote sensing will be examined. Second, some aspects of using fluorometry to quantify CDOM concentrations will be discussed. Third, the effect of CDOM fluorescence on CDOM absorption measurements made with diode array spectrophotometers and reflecting tube absorption meters will be examined.

Solar-induced CDOM fluorescence

The significant effect of CDOM absorption on the remote sensing of ocean color has been documented by many researchers (Bricaud et al., 1981; Prieur and Sathyendranath, 1981; Morel, 1988; Gordon et al., 1988; Carder et al., 1989, 1991). A question that has not been addressed in much detail is how much of an effect ambient CDOM fluorescence has on passive ocean color remote sensing signals. Spitzer and Dirks (1985) examined the problem theoretically using a two-flow irradiance model and fluorescence efficiency data from Zepp and Sholtzhauer (1981). They used a Φ_f of 0.0045 for all λ_x, which is a little less than half of the average values calculated in Part 1, and a Gaussian emission curve (plotted versus λ_m)

centered at 450 nm. They calculated the ratio $R_f(\lambda)/R(\lambda)$ where $R(\lambda)$ is the irradiance reflectance ($E_u(\lambda)/E_d(\lambda)$ = upwelling irradiance/downwelling irradiance) just below the sea surface and $R_f(\lambda)$ is the contribution to $R(\lambda)$ that results from CDOM fluorescence. For a pigment concentration, P (= $<Chl_a>$ + $<pheo_a>$), of 1 mg/m^3 they calculated that R_f/R at 450 nm was about 0.1, 0.3, and 0.7 for waters with CDOM absorption coefficients at 350 nm ($a_{cdom}(350)$) of 1.5, 4.5, and 10.5 m^{-1}, respectively, and that $R_f(\lambda)/R(\lambda)$ was < 0.1 at 520 nm and 550 nm. For comparison, $a_{cdom}(350)$ is typically 1 to 5 m^{-1} in Tampa Bay, is usually < 1 m^{-1} in coastal areas not heavily influenced by terrestrial discharge, and is < 0.1 m^{-1} for clear waters such as the Loop Current. If their calculations are accurate, CDOM fluorescence might contribute half the upwelling irradiance at the surface in highly colored waters, indicating a clear need to investigate this effect further.

In this section, $R_f(\lambda)$ and $R(\lambda)$ are calculated for 4 stations along a transect off Tampa Bay, Florida using both a simple radiative transfer model developed here and a slightly modified version of the Spitzer and Dirks (SD) model. Both models assume a homogeneous and optically deep water column. Only scattered light and light fluoresced by CDOM were considered to contribute to $R(\lambda)$, i.e. effects due to bottom reflectance, water Raman scattering, etc. have been neglected. A discussion of some of these effects can be found in Lee et al. (1992). The same input parameters are used for both models and the results are compared.

Simple model

The simple model is described by the following equations:

$$R(\lambda_m) = R_s(\lambda_m) + R_f(\lambda_m) \tag{12}$$

$$R_s(\lambda_m) = .33\ b_b(\lambda_m) \,/\, (a(\lambda_m) + b_b(\lambda_m)) \tag{13}$$

$$R_f(\lambda_m) = \frac{D_d}{2\ E_d(0-,\lambda_m)} \int \frac{E_d(0-,\lambda_x)\ a_{cdom}(\lambda_x)\ \eta(\lambda_x,\lambda_m)}{K_d(\lambda_x) + K_{u,f}(\lambda_m)}\ d\lambda_x \tag{14}$$

Eq. 13 is from Morel and Prieur (1977), and Eq. 14 is derived in Appendix 2. R_s = reflectance just below the sea surface due to scattered light, $K_d = D_d(a+r_d b_b)$, $K_{u,f} = D_{u,f}(a+r_{u,f} b_b)$, $a = a_w + a_p + a_{cdom}$, and $b_b = b_{bw} + b_{bp}$ (the λ dependencies have been left out in the text for brevity). a is the absorption coefficient, b_b is the backscattering coefficient, and the subscripts 'w' and 'p' refer to water and particles. D is the distribution function, which represents the increased probability of absorption or scattering due to the average increase in pathlength per unit depth for photons traveling at angles away from vertical, and it is thus a function of the angular distribution of the light field. r is the backscattering shape factor which converts the backscattering probability into a probability that a scattered photon will end up in the downwelling or upwelling light stream, and it too depends on the angular distribution of the light field (see Stavn and Weidemann, 1989). D and r are assumed to be constant with respect to λ. The subscripts 'd,' 'u,' and 'f' refer to downwelling, upwelling, and pertaining to fluorescence, respectively. $E_d(0-)$ is the spectral

downwelling solar irradiance just below the sea surface in terms of quantum flux (e.g. quanta/cm^2-sec-nm) rather than energy flux (e.g. watts/cm^2-nm).

SD model

The two-flow irradiance model of Spitzer and Dirks (1985) is modified in two ways. First, their CDOM fluorescence term, a Gaussian curve with maximum emission at 450 nm and a $\Phi_f(\lambda_x)$ of 0.0045, is replaced by measured $\eta(\lambda_x,\lambda_m)$ functions. Second, the backscattering coefficients have been multiplied by shape factors, a detail that their original model did not take into account.

Model inputs for West Florida Shelf transect

Optical measurements were taken along a transect from the mouth of Tampa Bay to the mid-West Florida Shelf on 4-5 March 1990 (see Figure 6) at Stations 1 through 4. FA and HA were extracted from Station 4, which corresponds to samples FA7 and HA6, and from Station 7, which corresponds to samples FA8 and HA8 (also HA4 from an earlier cruise). $\eta(\lambda_x,\lambda_m)$ for CDOM at Station 1 and Station 4 were calculated via Eq. 10 assuming f = 0.9, with the measured FA and HA $\eta(\lambda_x,\lambda_m)$ values from Station 7 used as surrogates for Station 1 data. $\eta(\lambda_x,\lambda_m)$ for CDOM for Stations 2 and 3 were taken to be an average of the two end point stations. a_w and b_{bw} were obtained from the tables in Smith and Baker (1981), a_p and a_{cdom} were

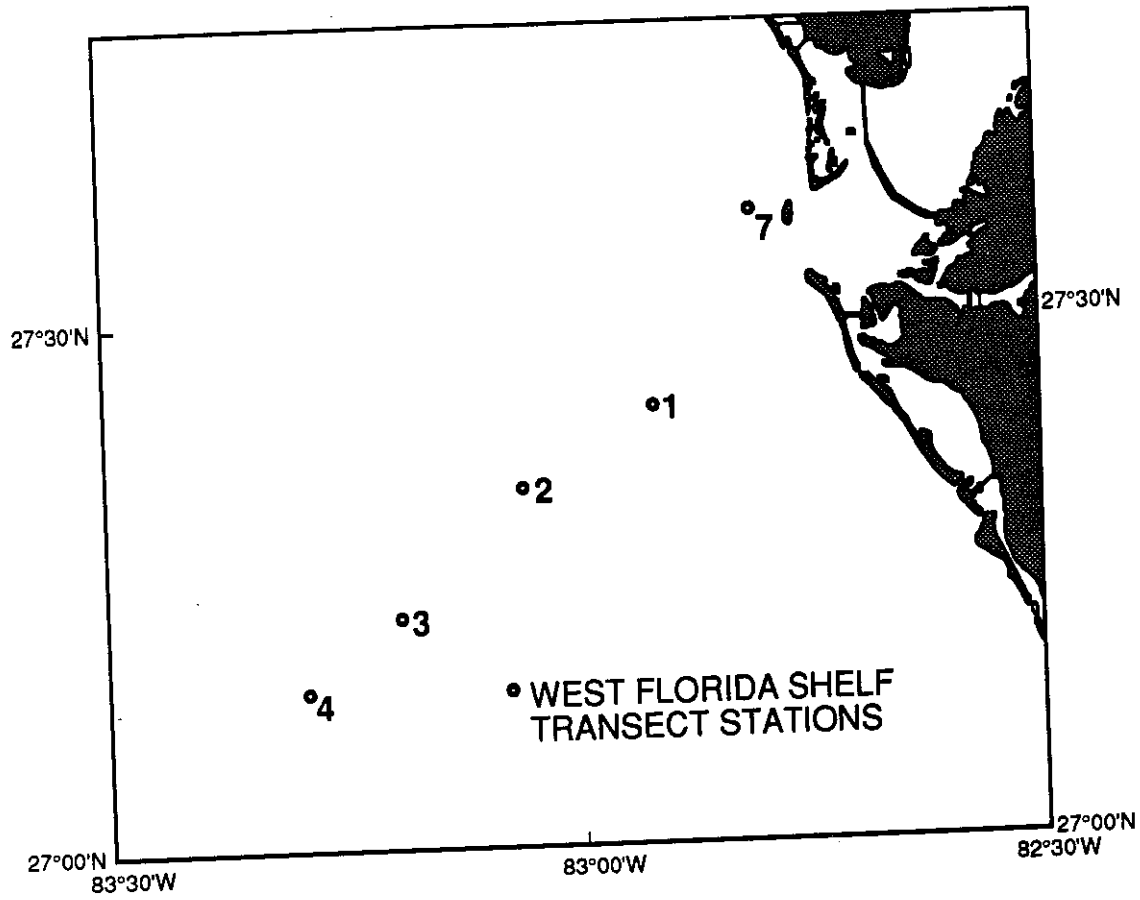

Figure 6. Station locations for the West Florida Shelf transect.

measured on the cruise at each station, and b_{bp} was estimated as a function of pigment concentration, P, using a model taken from Morel (1988). D_d = 1.14-1.22, calculated according to the solar zenith angle using the formulation of Prieur and Sathyendranath (1981), $D_{u,f}$ = 2.0, calculated assuming the fluoresced irradiance is isotropic, r_d = 1.09-1.18, calculated based on the San Diego Harbor volume scattering function measured by Petzold (1972) and D_d, and $r_{u,f}$ = 1.76, calculated based upon the same volume scattering function and an isotropic upwelling radiance distribution. $E_d(0-)$ is calculated from the RADTRAN irradiance model (Gregg and Carder, 1991). Other station information is listed in Table 4.

Model results and discussion

The results for all four stations are shown in Figure 7 for the simple model and in Figure 8 for the SD model as a) $R_f(\lambda)$ and b) the ratio $R_f(\lambda)/R(\lambda)$. The maximum effect for these waters is at 520 nm, where R_f/R is around 0.085 at Station 1 and about 0.065 at Stations 2, 3, and 4, and R_f/R is at least 0.020 for most of the visible range. Spitzer and Dirks' original study found more of a fluorescent contribution at 450 nm than in the green because their fluorescence emission curves had maxima at 450 nm, while the measured $\eta(\lambda_x,\lambda_m)$ curves used here have maxima as far out as 550 nm for λ_x = 490 nm. The two models yield quantitatively and spectrally similar results, and the remainder of the discussion will focus on the results from the simple model.

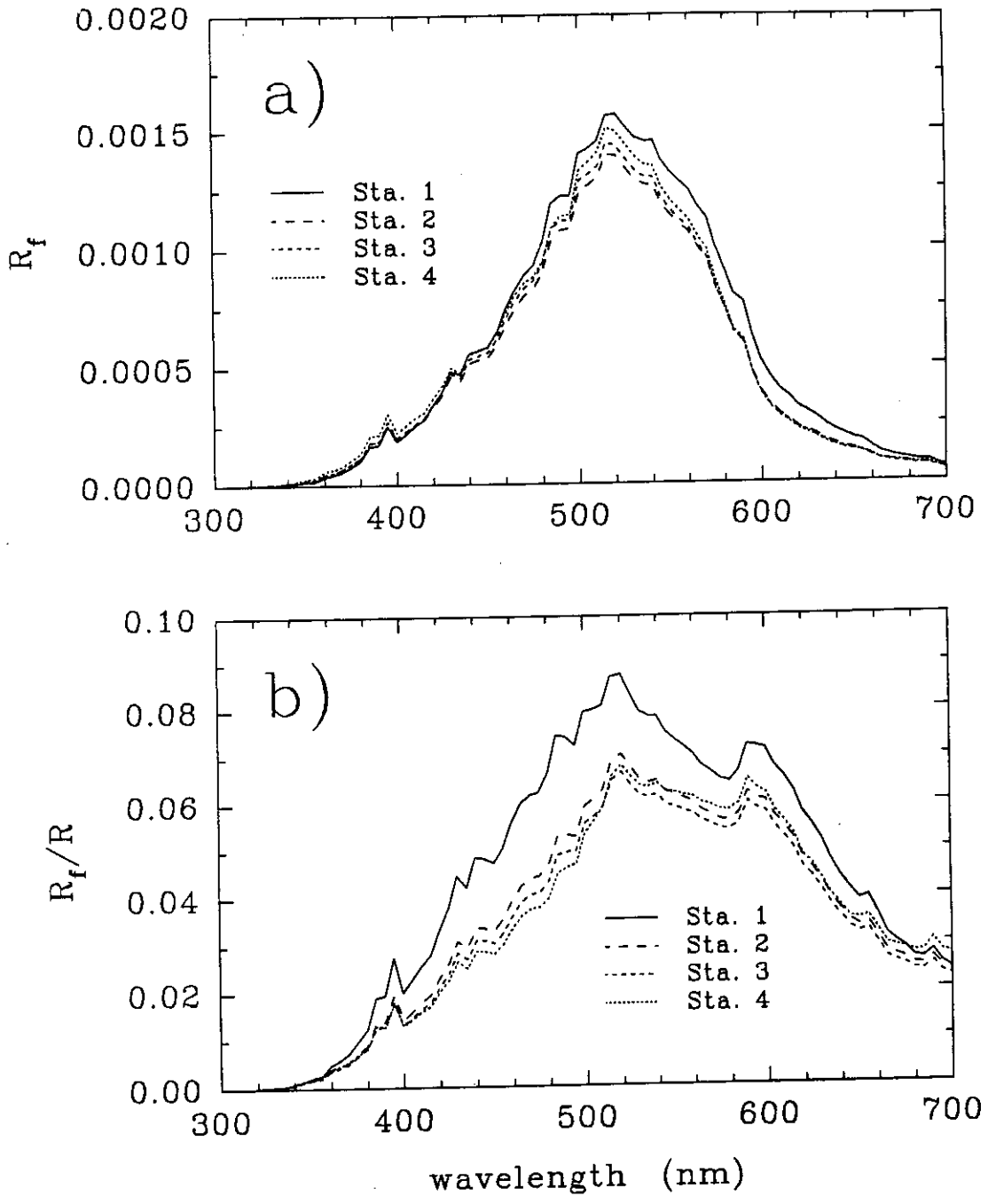

Figure 7. Reflectance spectra calculated using the Simple model. a) $R_f(\lambda)$, added reflectance due to CDOM fluorescence. b) $R_f(\lambda)/R(\lambda)$, added reflectance due to CDOM fluorescence as a fraction of the total reflectance.

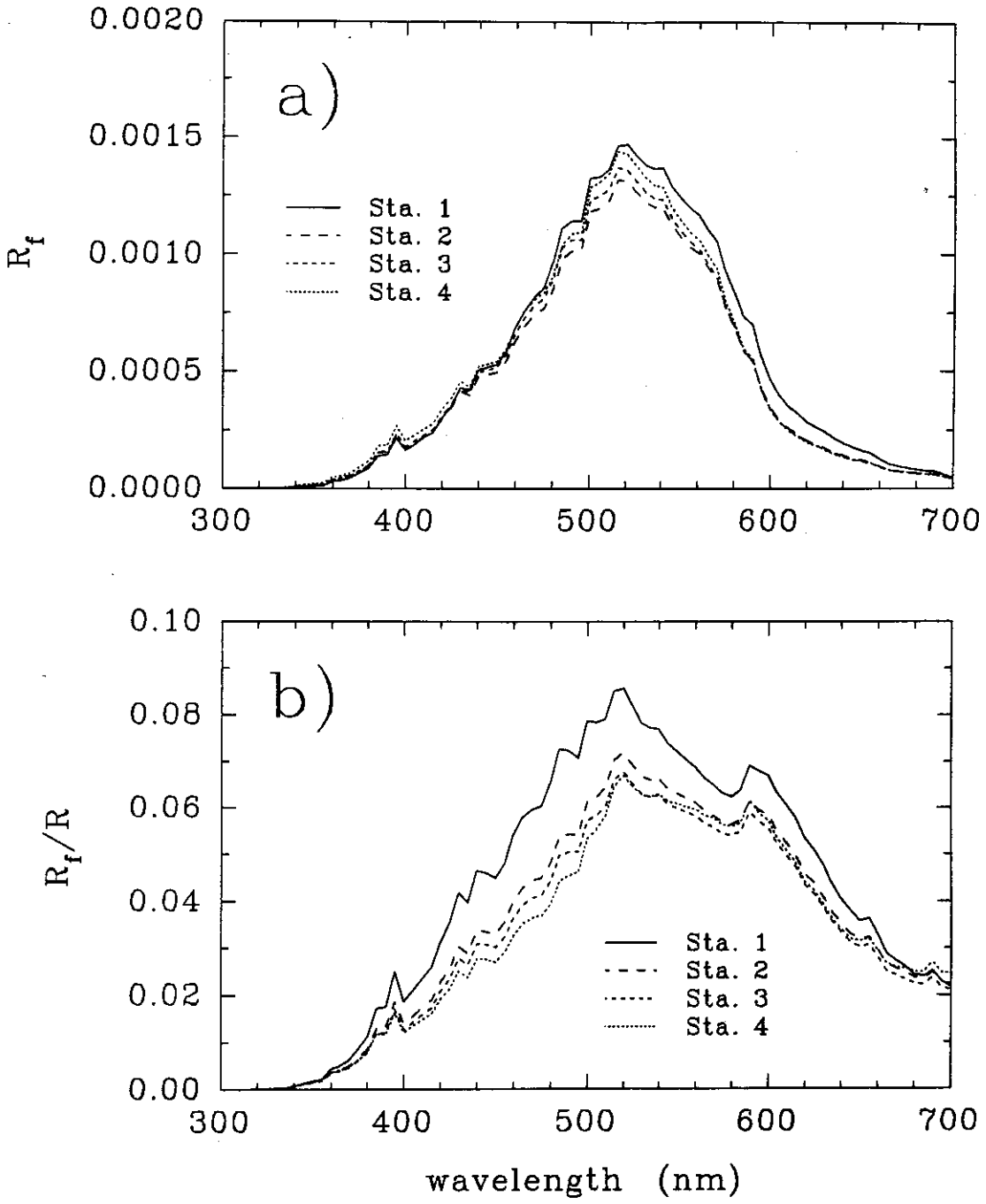

Figure 8. Reflectance spectra calculated using the SD model. a) $R_f(\lambda)$, added reflectance due to CDOM fluorescence. b) $R_f(\lambda)/R(\lambda)$, added reflectance due to CDOM fluorescence as a fraction of the total reflectance.

Effects on CZCS-type pigment algorithms. For coastal areas with even moderate amounts of CDOM, the CDOM fluorescence contribution to $R(\lambda)$ can be as large as 8.5%, and this contribution occurs at wavelengths important to ocean color remote sensing (e.g. 520 nm and 550 nm). The effect of this added irradiance on CZCS-type pigment algorithms (which are based on ratios of two radiance or irradiance measurements made at different wavelengths; see Gordon and Morel, 1983) will be negligible if 1) the magnitude of CDOM fluorescence covaries with pigment concentration, which will cause its fluctuations to be incorporated into empirical constants, or if 2) $R_f(\lambda)/R(\lambda)$ is about the same at the two wavelengths being ratioed. For $P > 1.5$ mg/m^3, an algorithm using the ratio R(520)/R(560) is typically used, and it appears from Figures 7b and 8b that condition 2) above holds. However, for $P < 1.5$ mg/m^3, the ratio R(440)/R(560) is typically used and neither of the above conditions is obviously applicable.

For the purpose of estimating the maximum error in pigment concentration estimates due to CDOM fluorescence, the algorithm $P_{alg} = 1.71\ [R(440)/R(560)]^{-1.82}$ (mg/m^3) was chosen (Gordon and Morel, 1983). The maximum error is estimated by the ratio P'_{alg}/P_{alg}, where P'_{alg} is calculated via the chosen algorithm using modeled reflectance values that include CDOM fluorescence (i.e. $R(\lambda)$ from the simple model) and P_{alg} is calculated using modeled reflectance values that do not include fluorescence (i.e. $R_s(\lambda)$ from the simple model). The results are listed in Table 5. Since the CZCS-type pigment estimates will only be affected to the extent that the fluorescent signal does not covary with actual pigments, $P'_{alg}/P_{alg}-1$ can be taken as an upper

Table 5. West Florida Shelf transect station information and pigment algorithm results. P_{mea} is the measured pigment concentration (<Chl *a*> + <pheo *a*>), P_{alg} is the pigment concentration calculated via a commonly used CZCS-type algorithm using reflectance values derived from the simple model without fluorescence as input, and P'_{alg} is the same as P_{alg} except that fluorescence is included in the calculated reflectance values.

Sta. #	sun angle (deg)	$a_{cdom}(350)$ (m^{-1})	P_{mea} (mg/m^3)	P_{alg} (mg/m^3)	P'_{alg}/P_{alg}
1	49.6	0.624	2.43	3.77	1.048
2	36.0	0.347	1.65	2.21	1.057
3	39.7	0.329	1.71	1.99	1.056
4	53.4	0.267	1.35	1.52	1.065

bound for errors induced by CDOM fluorescence. From Table 5, we see that the error in P estimates for these waters is probably < 5% (overestimate), with the greater potential errors found in waters with lower pigment concentration.

Although P_{alg} is up to 55% higher than the measured pigment concentration, P_{meas} (see Table 5), the point of this exercise is to examine possible errors due solely to CDOM fluorescence, and the magnitude of P is only of minor importance. This error in the CZCS algorithm is possibly due to unusually high chlorophyll-specific absorption coefficients for the phytoplankton in the study area (Lee et al., 1992), and perhaps due to a higher CDOM:chlorophyll ratio than was present in the data sets used to develop the CZCS algorithm (see Carder et al., 1991)

Remote-sensing reflectance vs. irradiance reflectance. The CDOM fluorescence contribution can be even higher for remote-sensing reflectance, $R_{rs} = L_w(\theta,\phi)/E_d$, than for the irradiance reflectance, $R = E_u/E_d$, depending on the direction of observation of $L_w(\theta,\phi)$ determined by the zenith angle θ and the azimuth angle ϕ. $L_w(\theta,\phi)$ is the upwelling *radiance* just above the sea surface (a.k.a. the water-leaving radiance), and E_u is the upwelling *irradiance* just below the sea surface. Radiance is a measure of the radiant flux for photons traveling in a given direction within a given small solid angle, whereas upwelling (or downwelling) irradiance is a measure of the radiant flux for photons traveling at all upward (or downward) traveling angles weighted by the cosine of the zenith angle. The distinction between R_{rs} and R is important because satellite and airborne spectrometers measure $L_w(\theta,\phi)$, not E_u. The

following is a conceptual argument demonstrating that $L_w(\theta,\phi)$, as measured by the CZCS, is likely to have a higher contribution from CDOM fluorescence than is E_u at a given site. The spectral dependencies have been excluded for brevity and the depth dependencies for the reflectance, radiance, and irradiance paramenters are stated explicitly in the text.

The CZCS measures $L_w(\theta,\phi)$ (after corrections to remove atmospheric effects) in the above-surface zenith angle range of $\theta \approx 0°$-$40°$ and the azimuth angle can be ignored, so we will drop the ϕ dependency. To compare $L_w(\theta)$ and E_u, we first pass $L_w(\theta)$ through the air-sea interface to get $L_u(\theta)$, the upwelling radiance just below the sea surface. In so doing, the below-surface zenith angle range viewed by the CZCS is reduced to $\theta \approx 0°$-$29°$. Next, we estimate the CDOM fluorescence contribution to $L_u(\theta)$ and E_u by the ratios $L_{u,f}(\theta)/L_u(\theta)$ and $E_{u,f}/E_u$, where the subscript 'f' refers to radiance or irradiance originating from fluorescence. Finally, the irradiance contribution ratio can be written in terms of the corresponding radiances as

$$\frac{E_{uf}}{E_u} = \frac{\int_{2\pi} L_{uf}(\theta)\cos\theta \; d\omega}{\int_{2\pi} L_u(\theta)\cos\theta \; d\omega} \tag{15}$$

Next, consider Figure 9. Figure 9a shows an azimuthally averaged upwelling radiance distribution, $L_u(\theta)$, at 4 m depth taken from Tyler (1960). $L_u(\theta)$ is larger at angles away from vertical than it is at or near vertical. This phenomenon is described as "limb-brightening" and it is typical of $L_u(\theta)$ distributions in natural waters. Figure 9b shows an upwelling radiance distribution for CDOM fluorescence,

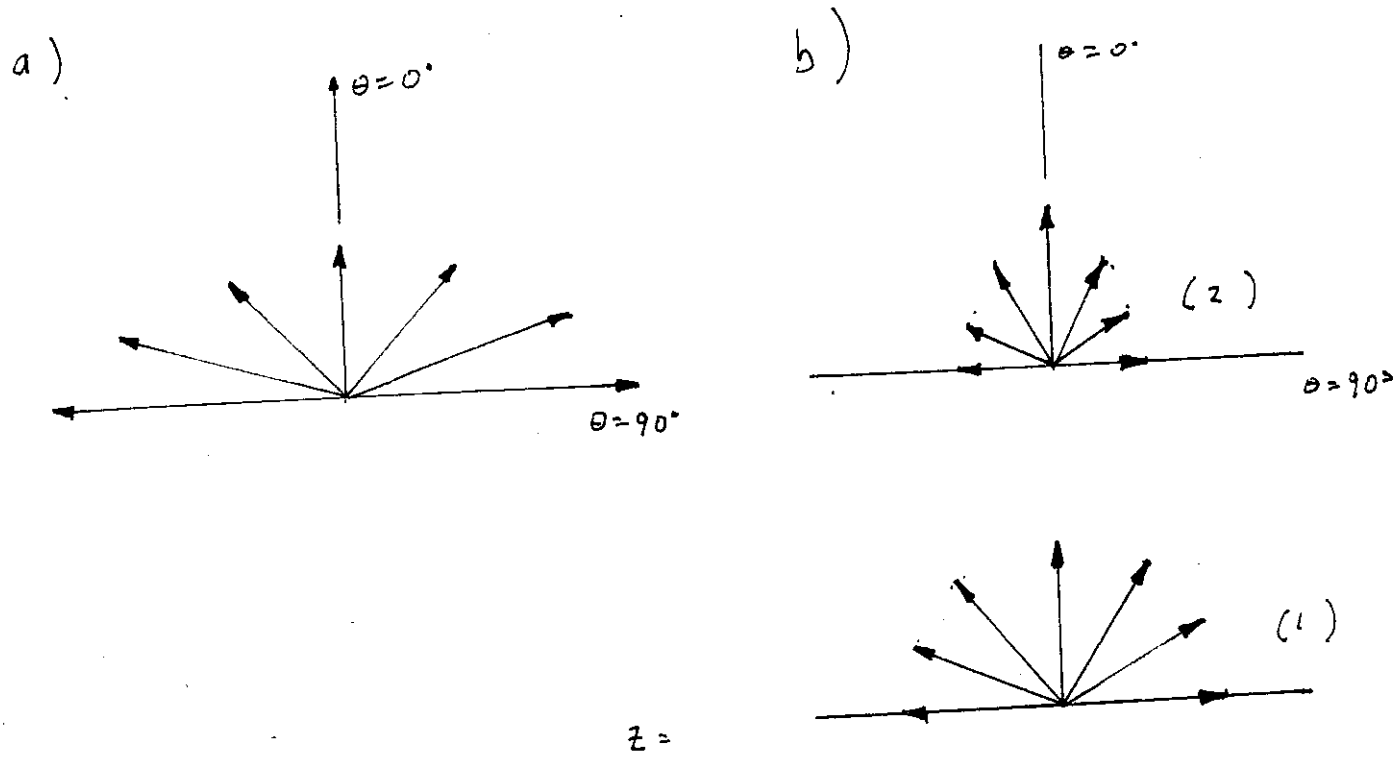

Figure 9. Schematic diagrams of relative upwelling radiance distributions for a) total and b) fluoresced radiance. a) "Limb-brightened" upwelling radiance distribution, $L_u(\theta)$, at 4.24 m depth in Lake Pend Orielle, from Tyler (1960). Azimuth angle = 90°, λ = 480 nm. b) Upwelling radiance distribution for fluoresced radiance which is initially isotropic (1). Traveling up the water column, attenuation is greater at angles away from vertical, so that near the surface, the fluoresced upwelling radiance distribution, $L_{u,f}(\theta)$ is "limb-darkened" (2).

$L_{u,f}(\theta)$, which is equal in all directions at the point of fluorescence at depth (1). As $L_{u,f}(\theta)$ travels upward through the water column, radiance traveling at angles away from vertical will be attenuated more strongly due to the increased length of the slanted path. As a result, $L_{u,f}(\theta)$ just below the sea surface will be larger at vertical than it is at angles away from vertical (2), a phenomenon described as "limb-darkening."

We can see that $L_{u,f}(\theta)/L_u(\theta)$ for $\theta = 0°$-$29°$ will be larger than $E_{u,f}/E_u$ by looking at Eq. 15 and Figure 9 together. First, from Eq. 15 we need to integrate $L_{u,f}(\theta)$ and $L_u(\theta)$ over the entire 2π upwelling hemisphere to get $E_{u,f}/E_u$. Second, by looking at Figure 9 and assuming that the azimuthal dependencies of $L_{u,f}(\theta)$ and $L_u(\theta)$ are small, we can see that the contribution to $E_{u,f}$ by the limb-darkened $L_{u,f}(\theta)$ at zenith angles $\theta > 29°$ will be less than the contribution to E_u by the limb-brightened $L_u(\theta)$ at those same angles. Thus, the contribution to $L_u(\theta)$ by CDOM fluorescence for $\theta = 0°$-$29°$, which is equivalent to the contribution to $L_w(\theta)$ for $\theta = 0°$-$40°$, will be greater than the CDOM fluorescence contribution to E_u. Any other isotropic light source, such as water Raman scattering or pigment fluorescence, will similarly contribute more to $L_w(\theta)$ than to E_u. The implications of this excercise are that 1) remotely sensed radiances will be even more susceptible to CDOM fluorescence contamination than is indicated by the irradiance model calculations done above, and 2) caution must be used when employing R as a proxy for R_{rs} in modeling fluorescence effects on remotely sensed radiance.

Fluorometric detection of FA and HA

CDOM fluorescence has frequently been used as a means of assessing DOC with varying degrees of success (Smart et al., 1976; Stewart and Wetzel, 1981; references in Coble, 1992). Most of the attempts rely on statistical regression of measured fluorescence vs. measured DOC over a given study area, which may become invalid if a^* or $\eta(\lambda_x,\lambda_m)$ for CDOM, or the DOC:CDOM ratio changes over the study area. Possible mechanisms for such a change include biological production or photo-bleaching of CDOM, or mixing with a water source that was not accounted for in the original regression. Although other mechanisms may also act to decrease the validity of the statistical regression approach, accounting for variability in a^*_{cdom} and $\eta(\lambda_x,\lambda_m)$ can eliminate two potential sources of error.

The problem can be approached as follows. CDOM concentration, C_{cdom}, can be related to a remotely sensed fluorescence signal, $F(\lambda_m)$, via $F(\lambda_m) = I(\lambda_x,\lambda_m)\ C_{cdom}\ a^*_{cdom}(\lambda_x)\ \eta(\lambda_x,\lambda_m)$, where $I(\lambda_x,\lambda_m)$ is an instrumental constant that can be determined in calibration. If $a^*(\lambda_x)$ and $\eta(\lambda_x,\lambda_m)$ are not known *a priori*, they can be measured at two endpoints of an inshore/offshore transect and their gradients estimated. $F(\lambda_m)$ can be measured via either airborne LIDAR or by an *in situ* fluorometer towed by a ship, and converted to C_{cdom} if the instrument has been properly calibrated and if the estimated gradients of $a^*(\lambda_x)$ and $\eta(\lambda_x,\lambda_m)$ along the flight/ship track are accurate. If DOC concentrations are desired, the conversion factor DOC/C_{cdom} must be determined. Data for the Mississippi outflow region from Harvey et al. (1983), yield

an average DOC/C_{cdom} value of 1.36 (n=3, σ_n=0.45), assuming CDOM = FA + HA. These numbers are based upon UV-oxidation methods, thought to be low relative to platinum catalytic measurements of DOC (Sugimura and Suzuki, 1988; Williams and Druffel, 1988). Few other data exist, and this ratio is probably highly variable from region to region, thus requiring that site-specific values be determined.

If variability in $\eta(\lambda_x,\lambda_m)$ is not accounted for, we can calculate the additional error in C_{cdom} estimates by examining the appropriate wavelength regions of the $\eta(\lambda_x,\lambda_m)$ surfaces. For example, consider a LIDAR instrument, validated at Station 1 of the West Florida Shelf transect (see Figure 6), using a 355 nm laser excitation source and a 10 nm bandwidth receiver centered on 490 nm. η(355,485-495) is 11% higher at Station 4 than at Station 1, which will cause an 11% overestimate of C_{cdom} if variability in $\eta(\lambda_x,\lambda_m)$ is not accounted for. However, if λ_x/λ_m for the system can be changed to 390/440-490 nm, the overestimate due to variability in η is reduced to about 3%.

It may also be possible to determine C_{cdom} from remotely sensed fluorescence by radiative transfer modeling or by Monte Carlo simulation (see Poole and Esaias, 1981). In either case, the $\eta(\lambda_x,\lambda_m)$ measurements presented in Part 1 provide examples of the quantitative fluorescence data that are required for such analytical methods to be employed.

Absorption measurements

Most conventional spectrophotometer measurements are relatively free of contamination by fluorescence of the sample because they employ a monochromatic light source, which yields a small excitation energy, and the solid angle of collection by the detector from the sample is small, excluding most of the isotropically fluoresced radiance. Short sample pathlengths will further decrease the amount of fluorescence. Here the effects of CDOM fluorescence on absorption measurements made in diode array spectrophotometers, which have small acceptance angles but panchromatic excitation light, and in reflecting tube absorption meters, which have a monochromatic light source but potentially large acceptance angles and long pathlengths, are investigated using the $\eta(\lambda_x,\lambda_m)$ measurements made in Part 1.

Diode array spectrophotometers

Diode array spectrophotometers measure absorption spectra by passing panchromatic radiance through a sample and dispersing the transmitted light via a diffraction grating onto a linear array of photodiodes. Absorption is thus measured at hundreds of wavelength intervals at once. Both the solid angle of collection and the pathlength within the sample (typically 1 cm) are small, but since the light source is panchromatic, a large section of the incident spectrum is available to excite fluorescence. A model was developed to calculate the effect of the added

fluorescence on absorbance (A) so that the results can be compared to typical instrument specifications.

Absorbance model. The model calculates the absorbance of a sample with no fluorescence effects added as $A(\lambda) = A_w(\lambda) + A_{cdom}(\lambda)$, where the subscripts 'w' and 'cdom' refer to water and CDOM, respectively (the effect of particles was neglected). The absorbance measured by the spectrophotometer with CDOM fluorescence effects added, $A'(\lambda)$, is calculated by

$$A'(\lambda_m) = \log\left[\frac{1}{T(\lambda_m) + T_f(\lambda_m)}\right] \tag{16}$$

where $T(\lambda_m) = 10^{-A(\lambda m)}$ is the transmittance of the sample and $T_f(\lambda_m)$ is the added effect on transmittance due to CDOM fluorescence, calculated by

$$T_f(\lambda_m) = \frac{1}{E_0(\lambda_m)} \frac{\omega}{4\pi} \int_{\lambda_x} E_0(\lambda_x)(1-10^{-A_{cdom}(\lambda_x)})\, \eta(\lambda_x,\lambda_m)\, d\lambda_x \tag{17}$$

where ω is the solid angle of collection in radians, $E_0(\lambda)$ is the incident irradiance in relative quantum flux units, and the integration is carried out from 310 nm to λ_m or 490 nm, whichever value is lower, since this is the range of λ_x for which $\eta(\lambda_x,\lambda_m)$ measurements are available. The derivation of this model is explained in Appendix 3.

$A_w(\lambda)$ and $A_{cdom}(\lambda)$ are calculated via $A(\lambda) = a(\lambda)\, l/2.303$, where $a(\lambda)$ is the absorption coefficient in m^{-1}, and l is the pathlength, set to 1 cm. a_w was obtained from Smith and Baker (1981) and $a_{cdom}(\lambda) = a_{cdom}(350) \cdot \exp[-0.014(\lambda-350)]$. $a_{cdom}(350)$ was set to 0.5, 1.0, and 5.0 m^{-1} on each of three different runs of the

model. The spectral character of $E_0(\lambda)$ was that of a deuterium lamp, $\eta(\lambda_x,\lambda_m)$ was the same as that used in the solar-induced fluorescence section, and $\omega/4\pi$ was chosen to be 0.01.

Results. The results are shown in Figure 10 as $A(\lambda)$-$A'(\lambda)$. As can be seen, the maximum effect is about 0.0000045 absorbance units at 520 nm which is well below the detection limit of any commercially available spectrophotometer. It is possible that this effect may be higher because fluorescence arising from CDOM absorption at $\lambda_x < 310$ nm and > 490 nm was neglected in calculating $T_f(\lambda)$. However, the value of 0.01 chosen for $\omega/4\pi$ is probably much higher than the actual solid angle of collection, so the fluorescence contamination effect is in all likelihood less than that shown in Figure 10. Thus, even for samples with high CDOM (i.e. where $a_{cdom}(350) = 5\ m^{-1}$), CDOM fluorescence has an undetectable effect on absorption measured by diode array spectrophotometers.

Reflecting tube absorption meter

This type of absorption meter is similar to a typical spectrophotometer in that it has a monochromatic beam that passes through the axis of a cylidrical sample cell and the transmitted light is collected on the other end. The main differences are that the internal walls of the cylinder reflect nearly 100% of incident light and that a diffusing plate is fitted onto the detector end of the sample cylinder. The reflective

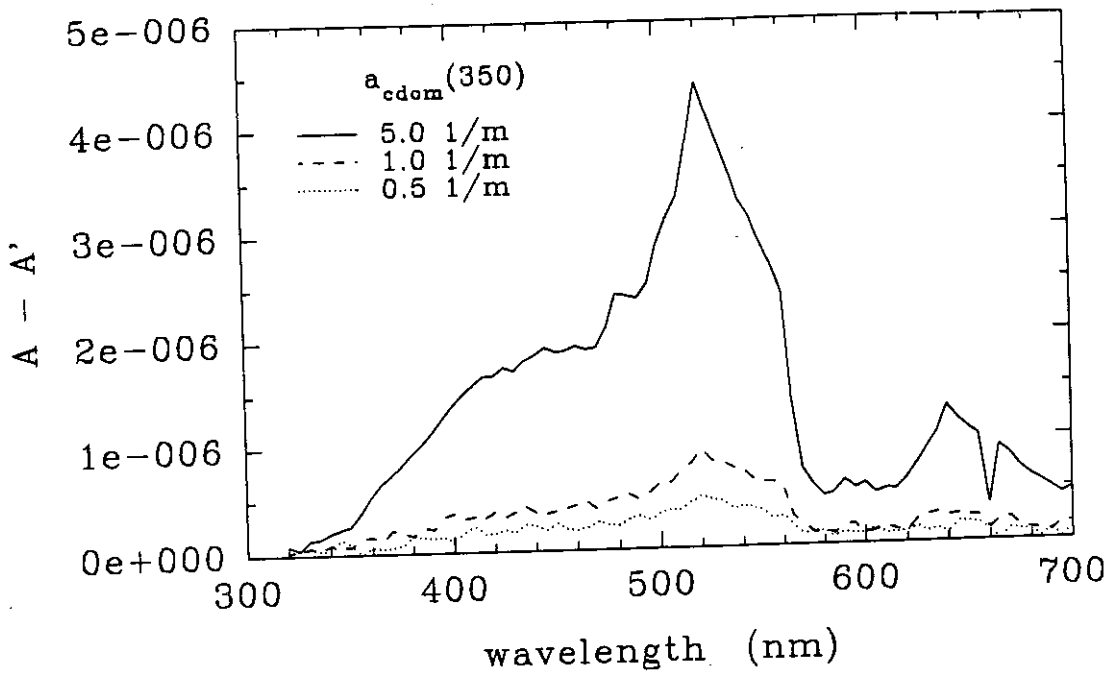

Figure 10. Decrease in absorbance measured by a diode array spectrophotometer due to CDOM fluorescence for $a_{cdom}(350)$ = 0.5, 1, and 5 m^{-1}. A is the actual absorbance of the sample and A' is the absorbance measured by the spectrophotometer with the effects of CDOM fluorescence included.

walls allow light scattered in a forward direction to be propagated down the tube by multiple reflection and the diffusing plate allows light incident within a given angle, θ_{max}, normal to the plate to be collected by the detector; thus, most of the light scattered at a forward angle $< \theta_{max}$ anywhere along the beam path will be collected and measured. Since most of the light scattered by marine particles is forward scattered within 45° to normal, a reflecting tube with $\theta_{max} = 45°$ measures all of the directly transmitted light and most of the scattered light. This yields a closer approximation to true absorption; if scattered light is not collected, the instrument measures attenuation (= absorption + scattering). A potential problem here is that any light fluoresced within the collection angle anywhere along the beam path will also be measured. A model was developed to calculate the added effect of this fluorescence on the transmittance of a sample so that the results can be compared to the specifications of a commercially available reflecting tube absorption meter (Zaneveld et al., 1990).

Transmittance model. The additional amount of transmittance due to CDOM fluorescence, $T_f(\lambda)$, measured by an instrument with a spectrally flat detector response is calculated by

$$T_f(\lambda_x) = \frac{\omega}{4\pi} a_{cdom}(\lambda_x) \int_{\lambda_x}^{700} \int_{0}^{L} \exp[-a(\lambda_x)x - a(\lambda_m)(L-x)/\mu] \cdot \eta(\lambda_x,\lambda_m)\, dx\, d\lambda_m \qquad (18)$$

where $a(\lambda) = a_w(\lambda) + P \cdot a^*_p(\lambda) + a_{cdom}(\lambda)$, $a^*_p(\lambda)$ is the pigment-specific absorption

coefficient for particles in m^2/mg, l is the pathlength within the sample in meters, x is distance along the beam path in meters, and μ is the average of $\cos\theta$ for all fluoresced photons within the detector collection angle i.e. for $\theta \leq \theta_{max}$ where θ is the angle of the fluoresced photon path relative to the cylinder axis. Other symbols have been defined previously. The derivation of this model is explained in Appendix 4.

Values for $a_w(\lambda)$, $a_{cdom}(\lambda)$, and $\eta(\lambda_x,\lambda_m)$ are as in the previous section. $a^*_p(\lambda)$ was taken from a measured value off Egmont Key, Florida, and l = 0.25 m. Assuming that $\theta_{max} = 45°$, we can calculate that $\omega/4\pi = 0.146$ and $\mu = 0.8535$ for isotropic radiance. Nine runs were made with three different values each for P (1, 4, and 10 mg/m^3) and $a_{cdom}(350)$ (0.5, 1, and 5 m^{-1}).

Results. The results are shown in Figure 11 where $T_f(\lambda)$ is shown for all nine runs. Pigment concentration has a negligible effect on $T_f(\lambda)$. For the highest CDOM concentration ($a_{cdom}(350) = 5\ m^{-1}$), contamination as high as 0.0011 units of transmittance can be found at $\lambda = 370$ nm where there is a local maximum in total fluorescence efficiency (Figure 3). This is well within the ± 0.0001 accuracy of a commercially available reflecting tube absorption meter that has the same pathlength and collection angle (Zaneveld et al., 1990).

Effect on absorption measurements. The fractional error in absorption due to the added fluorescence was calculated as $[a(\lambda)-a'(\lambda)]/a(\lambda)$, where $a'(\lambda)$ is the total measured absorption with fluorescence effects included, calculated by

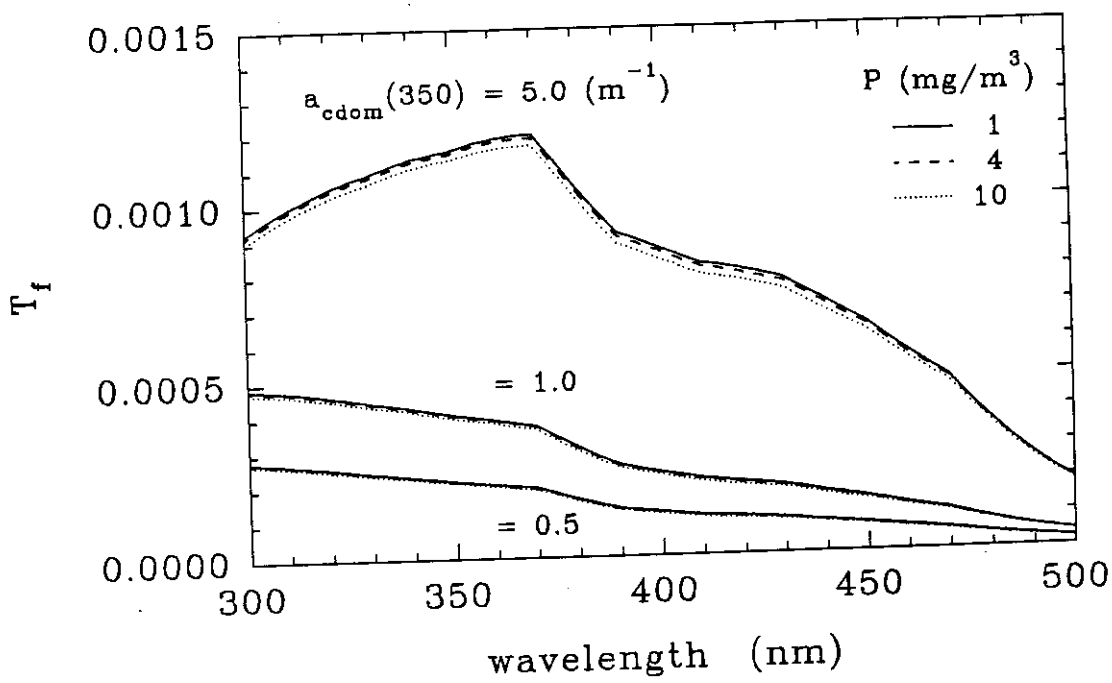

Figure 11. Increase in transmittance measured by a reflecting tube absorption meter due to CDOM fluorescence, T_f, for $a_{cdom}(350)$ = 0.5, 1, and 5 m^{-1} and P = 1, 4, and 10 mg/m^3.

$$a'(\lambda) = \frac{-\ln(T(\lambda) + T_f(\lambda))}{L} \qquad (19)$$

where $T(\lambda) = \exp[a(\lambda) \cdot l]$. The results are shown in Figure 12 for P = 1 and $a_{cdom}(350)$ = 0.5, 1, and 5 m^{-1}. The errors are everywhere on the order of a few tenths of a percent, with a maximum fractional error of about 0.0032 for the run with the highest CDOM for λ = 350-370 nm. This contamination will be larger if the detector collects longer wavelength photons more efficiently than shorter wavelengths, since the fluorescence contamination is of a longer wavelength than that being measured. It thus appears that reflecting tube absorption meters, unlike diode array spectrophotometers, can suffer from small but detectable errors due to CDOM fluorescence. Factors responsible for this are the large collection angle of the detector and the long sample pathlength.

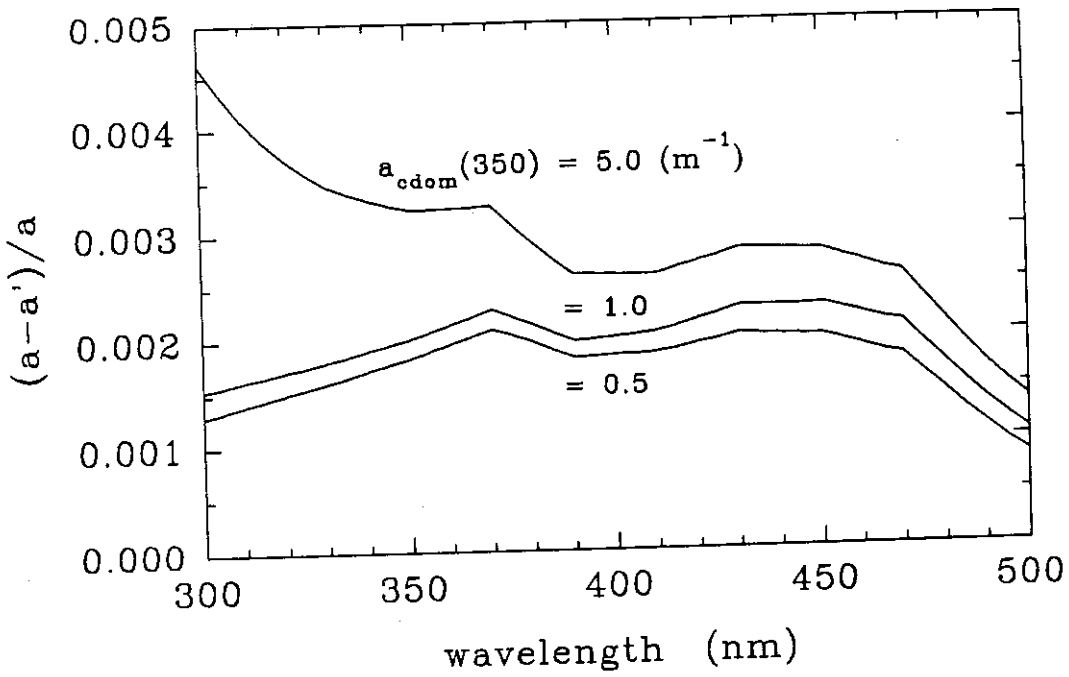

Figure 12. Fractional decrease in absorption measured by a reflecting tube absorption meter due to CDOM fluorescence for $a_{cdom}(350) = 0.5$, 1, and 5 m^{-1}. a is the actual absorption coefficient of the sample and a' is the absorption measured by the reflecting tube with CDOM fluorescence effects included.

PART 2 SUMMARY

1. For a coastal to mesotrophic transect off Tampa Bay, Florida (P = 2.43 to 1.35 mg/m^3), the percent contribution of CDOM fluorescence to R is broad-banded (about 200 nm half-bandwidth) with a maximum of about 6-8% at 520 nm. The effect of this added fluorescence on CZCS-type spectral ratio pigment algorithms is probably < 5%.

2. CDOM measurements based on remotely sensed fluorescence can be made more accurate if a^*_{cdom} and $\eta(\lambda_x,\lambda_m)$ for the given region are known *a priori* by eliminating the variability associated with these two parameters.

3. Absorption measurements made with diode array spectrophotometers are unaffected by CDOM fluorescence, whereas measurements made with reflecting tube absorption meters can suffer from a lowering of up to 0.32% for waters with $a_{cdom}(350) = 5\ m^{-1}$.

REFERENCES CITED

Aiken, G.R., Isolation and concentration techniques for aquatic humic substances, in *Humic Substances in Soil, Sediment, and Water*, eds. G.R. Aiken, D.M. McKnight, R.L. Wershaw, and P. MacCarthy, pp. 363-386, John Wiley and Sons, New York, 1985.

Aiken, G.R., Isolation of organic acids from large volumes of water by adsorption on macroporous resins, in *Organic Pollutants in Water: Sampling, Analysis, and Toxicity Testing*, eds. I.H Suffet and M. Malaiyandi, pp. 295-307, American Chemical Society, 1987.

Aiken, G.R., A critical evaluation of the use of macroporous resins for the isolation of aquatic humic substances, in *Humic Substances and Their Role in the Environment*, eds. F.H. Frimmel and R.F. Christman, pp. 15-28, John Wiley and Sons Ltd., 1988.

Amador, J.D., P.J. Milne, C.A. Moore, and R.G. Zika, Extraction of chromophoric humic substances from seawater, *Mar. Chem.*, 29, 1-17, 1991.

Bacastow, R., and E. Maier-Reimer, Dissolved organic carbon in modeling oceanic new production, *Glob. Biogeochem. Cycles*, 5, 71-86, 1991.

Berger, P., R.W.P.M. Laane, A.G. Ilahude, M. Ewald, and P. Courtot, Comparative study of dissolved fluorescenct matter in four West-European estuaries, *Oceanol. Acta*, 7, 309-314, 1984.

Black, A.P., and R.F. Christman, Characteristics of colored surface waters, *J. Am. Wat. Wks. Ass.*, 55(6), 753-770, 1963.

Bricaud, A., A. Morel, and L. Prieur, Absorption by dissolved organic matter in the sea (yellow substance) in the UV and visible domains, *Limnol. Oceanogr.*, 26, 43-53, 1981.

Cabaniss, S.E., and M.S. Shuman, Synchronous fluorescence spectra of natural waters: tracing sources of dissolved organic matter, *Mar. Chem.*, 21, 37-50, 1987.

Carder, K.L., R.G. Steward, G.R. Harvey, and P.B. Ortner, Marine humic and fulvic acids: Their effects on remote sensing of ocean chlorophyll, *Limnol.*

Oceanogr., 34, 68-81, 1989.

Carder, K.L., S.K. Hawes, K.A. Baker, R.C. Smith, R.G. Steward, and B.G. Mitchell, Reflectance model for quantifying chlorophyll *a* in the presence of productivity degradation products, *J. Geophys. Res.*, 96(C11), 20,599-20,611, 1991.

Carlson, R.E., and J. Shapiro, Dissolved humic substances: a major source of error in fluorometric analyses involving lake waters, *Limnol. Oceanogr.*, 26(4), 785-790, 1981.

Coble, P.G., Fluorescence of DOM: Implications for development of *in situ* instrumentation, in press in *Autonomous Bio-Optical Observing Systems Symposium Proceedings*, Monterey, CA April 6-10, 1992.

Coble, P.G., S.A. Green, N.V. Blough, and R.B. Gagosian, Characterization of dissolved organic matter in the Black Sea by fluorescence spectroscopy, *Nature*, 348, 432-435, 1990.

Coble, P.G., C.A. Schultz, and K. Mopper, Fluorescence contouring analysis of DOC intercalibration experiment samples: a comparison of techniques, in press in *Mar. Chem.*, 1992.

Donard, O.F.X., C. Belin, and M. Ewald, Corrected fluorescence excitation spectra of fulvic acids. Comparison with the UV/visible absorption spectra, *Sci. Total Env.*, 62, 157-161, 1987.

Donard, O.F.X., M. Lamotte, C. Belin, and M. Ewald, High sensitivity fluorescence spectroscopy of Mediterranean waters using a conventional or a pulsed excitation source, *Mar. Chem.*, 27, 117-136, 1989.

Ertel, J.R., and J.I. Hedges, Bulk chemical and spectroscopic properties of marine and terrestrial humic acids, melanoidins and catechol-based synthetic polymers, in *Aquatic and Terrestrial Humic Materials*, eds. R.F. Christman and E.T. Gjessing, pp. 143-163, Ann Arbor Science, Ann Arbor, 1983.

Ewald, M., C. Belin, and P. Berger, Corrected fluorescence spectra of fulvic acids isolated from soil and water, *Environ. Sci. Technol.*, 17(8), 501-504, 1983.

Ferrari, G.M., and S. Tassan, On the accuracy of determining light absorption by "yellow substance" through measurements of induced fluorescence, *Limnol. Oceanogr.*, 36(4), 777-786, 1991.

Ghassemi, M., and R.F. Christman, Properties of the yellow organic acids of natural waters, *Limnol. Oceanogr.*, 13, 583-597, 1968.

Gordon, H.R., The diffuse reflectance of the ocean: The theory of its augmentation by chlorophyll *a* fluorescence at 685 nm, *Appl. Opt.*, 18, 1161-1166, 1979.

Gordon, H.R., Ship perturbation of irradiance measurements at sea 1: Monte Carlo simulations, *Appl. Opt.*, 23, 4172-4182, 1985.

Gordon, H.R., Dependence of the diffuse reflectance of natural waters on the sun angle, *Limnol. Oceanogr.*, 34(8), 1484-1489, 1989.

Gordon, H.R., and A.Y. Morel, *Remote Assessment of Ocean Color for Interpretation of Satellite Visible Imagery*, 114 pp., Springer-Verlag, New York, 1983.

Gordon, H.R., O.B. Brown, R.H. Evans, J.W. Brown, R.C. Smith, K.S. Baker, and D. K. Clark, A semi-analytic model of ocean color, *J. Geophys. Res.*, 93, 10,909-10,924, 1988.

Gregg, W.W., and K.L. Carder, A simple 1 nm resolution solar irradiance model for cloudless maritime atmospheres, *Limnol. Oceanogr.*, 35, 1657-1675, 1990.

Harvey, G.R., Reply to: Comment on the structure of marine fulvic and humic acids, *Mar. Chem.*, 15, 89-90, 1984.

Harvey, G.R., D.A. Boran, L.A. Chesal, and J.M. Tokar, The structure of marine fulvic and humic acids, *Mar. Chem.*, 12, 119-132, 1983.

Hayase, K., and H. Tsubota, Sedimentary humic acid and fulvic acid as fluorescent organic materials, *Geochim. Cosmochim. Acta*, 49, 159-163, 1985.

Hedges, J.I., P.G. Hatcher, J.R. Ertel, and K.J. Meyers-Schulte, A comparison of dissolved humic substances from seawater with Amazon River counterparts by ^{13}C-NMR spectrometry, *Geochim. Cosmochim. Acta*, 56, 1753-1757, 1992.

Horth, H., rapporteur, et al., Environmental reactions and group report, in *Humic Substances and Their Role in the Environment*, eds. F.H. Frimmel and R.F. Christman, pp. 245-256, John Wiley and Sons Ltd., 1988.

Kalle, K., Uber das Verhalten und die Herkunft der in den Gewassern und in der Atmosphare vorhandenen himmelblauen Fluoreszenz, *Deutch. Hydrogr. Z.*, 16, 153-166, 1963.

Kester, D.R., I.W. Duedall, D.N. Connors, and R.M. Pytkowicz, Preparation of artificial seawater, *Limnol. Oceanogr.*, 12(1), 176-179, 1967.

Kirk, J.T.O., *Light and Photosynthesis in Aquatic Ecosystems*, 401 pp., Cambridge

University Press, Cambridge, 1983.

Kouassi, M., Light induced alteration of the photophysical properties of dissolved organic matter in seawater, M.S. Thesis, Univ. of Miami, Miami, 1986.

Laane, R.W.P.M., Composition and distribution of dissolved fluorescent substances in the Ems-Dollart Estuary, *Neth. J. Sea Res.*, 15(1), 88-99, 1981.

Laane, R.W.P.M., Comment on the structure of marine fulvic and humic acids, *Mar. Chem.*, 15, 85-87, 1984.

Lee, J.P., K.L. Carder, S.K. Hawes, R.G. Steward, T.G. Peacock, and C.O. Davis, An interpretation of high spectral resolution remote sensing reflectance, in *Ocean Optics XI*, Proc. SPIE, 1750, in press.

Leifer, A., *The Kinetics of Environmental Aquatic Photochemistry*, 304 pp., American Chemical Society, 1988.

Lewis, W.M., and D. Canfield, Dissolved organic carbon in some dark Venezuelan waters and a revised equation for spectrophotometric determination of dissolved organic carbon, *Arch. Hydrobiol.*, 79, 441-445, 1977.

Mantoura, R.F.C., and J.P. Riley, The analytical concentration of humic substances from natural waters, *Anal. Chim. Acta*, 76, 97-106, 1975.

Morel, A.Y., Optical modeling of the upper ocean in relation to its biogenous matter content (Case 1 waters), *J. Geophys. Res.*, 93, 10,749-10,768, 1988.

Morel, A.Y., and L. Prieur, Analysis of variations in ocean color, *Limnol. Oceanogr.*, 22, 709-722, 1977.

Muller-Wegener, U., Interaction of humic substances with biota, in *Humic Substances and Their Role in the Environment*, eds. F.H. Frimmel and R.F. Christman, pp. 179-192, John Wiley and Sons Ltd., 1988.

Petzold, T.L., Volume scattering functions for selected ocean waters, San Diego, Scripps Inst. Oceanogr., Ref. 72-78, 1972.

Pocklington, R., Chemical processes and interactions involving marine organic matter, *Mar. Chem.*, 5, 479-496, 1977.

Poole, L.R., and W.E. Esaias, Water Raman normalization of airborne fluorosensor measurements, *Appl. Opt.*, 21(20), 3756-3765, 1981.

Preisendorfer, R.W., and C.D. Mobley, Theory of fluorescent irradiance fields in natural waters, *J. Geophys. Res.*, 93(D9), 10,831-10,855, 1988.

Prieur, L., and S. Sathyendranath, An optical classification of coastal and oceanic waters based on the specific spectral absorption curves of phytoplankton pigments, dissolved organic matter, and other particulate materials, *Limnol. Oceanogr.*, 26, 671-689, 1981.

Reid, P.M., A.E. Wilkinson, E. Tipping, M.N. Jones, Determination of molecular weights of humic substances by analytical (UV scanning) ultracentrifugation, *Geochim. Cosmochim. Acta*, 54, 131-138, 1990.

Smart, P.L., B.L. Finlayson, W.D. Rylands, and C.M. Ball, The relation of fluorescence to dissolved organic carbon in surface waters, *Water Res.*, 10, 805-811, 1976.

Smith, R.C., and K.S. Baker, Optical properties of the clearest natural waters (200-800 nm), *Appl. Opt.*, 20, 177-184, 1981.

Spitzer, D., and R.W.J. Dirks, Contamination of the reflectance of natural waters by solar-induced fluorescence of dissolved organic matter, *Appl. Opt.*, 24(4), 444-445, 1985.

Stavn, R.H., Raman scattering effects at the shorter visible wavelengths in clear ocean waters, in *Ocean Optics X*, Proc. SPIE, 1302, pp. 94-100, 1990.

Stavn, R.H., and A.D. Weidemann, Shape factors, two-flow models, and the problem of irradiance inversion in estimating optical parameters, *Limnol. Oceanogr.*, 34(8), 1426-1441, 1989

Stewart, A.J., and R.G. Wetzel, Fluorescence:absorbance ratios: a molecular weight tracer of dissolved organic matter, *Limnol. Oceanogr.*, 25, 559-564, 1980.

Stewart, A.J., and R.G. Wetzel, Asymmetrical relationships between absorbance, fluorescence, and dissolved organic carbon, *Limnol. Oceanogr.*, 26(3), 590-597, 1981.

Stuermer, R.H., The characterization of humic substances in sea water, Ph.D. thesis, MIT/WHOI, Woods Hole, 1975.

Stuermer, R.H. and J.R. Payne, Investigation of seawater and terrestrial humic substances with carbon-13 and proton nuclear magnetic resonance, *Geochim. Cosmochim. Acta*, 40, 1109-1114, 1976.

Sugimura, T. and Y. Suzuki, A high temperature catalytic oxidation method for non-volatile dissolved organic carbon in seawater by direct injection of liquid samples, *Mar. Chem.*, 42, 105-131, 1988.

Thurman, E.M., and R.L. Malcolm, Preparative isolation of aquatic humic substances, *Environ. Sci. Technol.*, 15(4), 463-466, 1981.

Toggweiler, J.R., Is the downward dissolved organic matter flux important in carbon transport?, in *Productivity in the Ocean: Present and Past*, eds. W.H. Berger, V.S. Smetacek, and G. Wefer, pp. 65-83, John Wiley and Sons Ltd., 1989.

Tyler, J.E., Radiance distribution as a function of depth in an underwater environment, *Bull. Scripps Inst. Oceanogr.*, 7, 363-411, 1960.

Van Houten, J., and R.J. Watts, Temperature dependence of the photophysical and photochemical properties of the Tris(2,2'-bipyridyl)ruthenium(II) ion in aqueous solution, *J. Am. Chem. Soc.*, 98(16), 4853-4858, 1976.

Velapoldi, R.A., and K.D. Mielenz, A fluorescence standard reference material: quinine sulfate dihydrate, NBS special publication 260-64, 1980.

Visser, S.A., Fluorescence phenomena of humic matter of aquatic origin and microbial cultures, in *Aquatic and Terrestrial Humic Materials*, eds. R.F. Christman and E.T. Gjessing, pp. 183-202, Ann Arbor Science, Ann Arbor, 1983.

Walsh, J.J., K.L. Carder, and F.E. Muller-Karger, Meridional fluxes of dissolved organic matter in the North Atlantic Ocean, *J. Geophys. Res.*, 97(C10), 15,625-15,638, 1992.

Willey, J.D., The effect of seawater magnesium on natural fluorescence during estuarine mixing, and implications for tracer applications, *Mar. Chem.*, 15, 19-45, 1984.

Williams, P.M., and E.R.M. Druffel, Radiocarbon in dissolved organic matter in the central North Pacific Ocean, *Nature*, 330, 246-248, 1987.

Williams, P.M., and E.R.M. Druffel, Dissolved organic matter in the ocean: Comments on a controversy, *Oceanogr.*, 1, 14-17, 1988.

Yentsch, C.S., and C.M. Yentsch, Fluorescence spectral signatures: The characterization of phytoplankton populations by the use of excitation and emission spectra, *J. Marine Res.*, 37(3), 471-483, 1979.

Zaneveld, J.R., R. Bartz, and J.C. Kitchen, Reflective-tube absorption meter, in

Ocean Optics X, Proc. SPIE, 1302, pp. 124-136, 1990.

Zepp, R.G., Environmental processes involving natural organic matter, in *Humic Substances and Their Role in the Environment*, eds. F.H. Frimmel and R.F. Christman, pp. 193-214, John Wiley and Sons Ltd., 1988.

Zepp, R.G., and P.A. Schlotzhauer, Comparison of photochemical behavior of various humic substances in water: III. Spectroscopic properties of humic substances, *Chemosphere*, 10(5), 479-486, 1981.

Zika, R.G., Marine organic photochemistry, in *Marine Organic Chemistry: Evolution, Composition, Interactions, and Chemistry of Organic Matter in Sea Water*, eds. E.K. Duursma and R. Dawson, pp. 299-325, Elsevier, 1981.

APPENDICES

APPENDIX 1. NATURE OF THE 'WHITE FLOC' MATERIAL

Some of the extractions using C_{18} sorbent gave rise to a 'white floc' material upon elution. The white floc may result from a reaction of MeOH with ions in the $NaHCO_3$ solution (Nigel Simpson, Varian technical representative, personal communication) or it may be some of the C_{18} material itself, as the solid phase can degrade at a pH of about 2 or lower (Cynthia Moore, Univ. of Miami, personal communication). Absorption and fluorescence spectra were measured on white floc that had been dissolved in strong NaOH. The solution looked yellowish, and the absorption spectrum resembled a CDOM absorption curve that has other small peaks superimposed on top of it. The fluorescence emission spectrum had a peak at about 430 nm. The white color of the floc indicates that it is probably not aggregated humus - which would be yellow or brown - but it seems likely, based on the spectroscopic evidence, that at least some humics were taken out along with it when it precipitated.

Thus, the nature of the white floc material is still unclear. However, there was no white floc in the eluant from XAD-2 columns, and adequate extraction of humic substances by XAD-2 or XAD-8 resin has been documented by many researchers (Thurman and Malcolm, 1981; Aiken, 1987, 1988). Using XAD-type resins should eliminate the problem of the white floc material, although other problems, such as resin bleed and incomplete elution of extracted material, may still persist.

APPENDIX 2. DERIVATION OF $R_f(\lambda)$ FOR THE SOLAR-INDUCED CDOM FLUORESCENCE SECTION

The fraction of the irradiance reflectance just below the sea surface ($R(\lambda)$) that is due to CDOM fluorescence is designated as $R_f(\lambda)$. It is defined as $E_{u,f}(0-,\lambda)/E_d(0-,\lambda)$ where E is irradiance in quanta/cm^2-sec-nm, the subscripts 'u,' 'd,' and 'f' refer to upwelling, downwelling, and originating from fluorescence, respectively, and the '0-' indicates that the measurement is made just below the sea surface. Note that the depth dependencies have been dropped from $R(\lambda)$ and $R_f(\lambda)$ since we are only interested in their values just below the surface. Briefly, the derivation will consist of calculating $E_{u,f}(0-,\lambda)$ based on tracing a solar input spectrum down through the water column to a depth z where it is absorbed, fluoresced, and passed back up to the surface.

First, consider the solar irradiance at wavelength λ_x just below the surface, $E_d(0-,\lambda_x)$, and assume a homogeneous water column (i.e. all in-water properties are constant with respect to depth). The irradiance at depth z, $E_d(z,\lambda_x)$, is then

$$E_d(z,\lambda_x) = E_d(0-,\lambda_x)\, e^{-K_d(\lambda_x) z} \tag{20}$$

where $K_d(\lambda_x)$ is the downwelling diffuse attenuation coefficient in m^{-1}. The fraction of this irradiance that is absorbed by CDOM in the depth element dz is $a_{cdom}(\lambda_x) \cdot D_d(\lambda_x)$ where D_d is the distribution function for downwelling irradiance. D_d is equal to one over the average of $\cos\theta$ for all downwelling photons where θ is the angle the photon path makes with the downward vertical and it can be thought of as a path-lengthening

APPENDIX 2 (Continued)

effect. The fraction of this absorbed irradiance that is fluoresced in the upward direction at λ_m is equal to $1/2 \cdot \eta(\lambda_x,\lambda_m)$ assuming that the fluorescence is isotropic. Putting these factors together yields the upward fluoresced irradiance of wavelength λ_m originating from CDOM absorption at wavelength λ_x in the depth element dz at depth z, $E_{u,f}(z,\lambda_m)$:

$$dE_{u,f}(z,\lambda_m) = E_d(z,\lambda_x)\, a_{cdom}(\lambda_x)\, D_d(\lambda_x)\frac{1}{2}\,\eta(\lambda_x,\lambda_m)\, dz \qquad (21)$$

As the fluoresced irradiance travels up to the surface, it is attenuated by a factor $\exp[-K_{u,f}(\lambda_m) \cdot z]$ where $K_{u,f}$ is the diffuse attenuation coefficient for upwelling fluoresced irradiance in m^{-1}. Substituting Eq. 20, the fluoresced irradiance just below the sea surface, $E_{u,f}(0-,\lambda_m)$, originating from the depth element dz at depth z is then

$$dE_{u,f}(0-,\lambda_m) = \frac{1}{2}\, E_d(0-,\lambda_x)\, a_{cdom}(\lambda_x)\, D_d(\lambda_x)\cdot \eta(\lambda_x,\lambda_m)\, e^{-[K_d(\lambda_x)+K_{u,f}(\lambda_m)]z}\, dz \qquad (22)$$

Integrating this irradiance from $z = 0$ to ∞ yields

$$E_{u,f}(\lambda_m) = \frac{E_d(0-,\lambda_x)\, a_{cdom}(\lambda_x)\, D_d(\lambda_x)\, \eta(\lambda_x,\lambda_m)}{2\,[K_d(\lambda_x) + K_{u,f}(\lambda_m)]} \qquad (23)$$

$E_{u,f}(0-,\lambda_m)$ here represents the irradiance just below the sea surface that originates from CDOM fluorescence due to excitation at λ_x. In order to get the total fluoresced irradiance, we need to integrate over all λ_x. Then, assuming that D_d is independent of

APPENDIX 2 (Continued)

λ_x and dividing both sides by $E_d(0-,\lambda_m)$ yields

$$R_f(0-,\lambda_m) = \frac{D_d}{2\,E_d(0-,\lambda_m)} \int \frac{E_d(0-,\lambda_x)\, a_{cdom}(\lambda_x)\, \eta(\lambda_x,\lambda_m)}{K_d(\lambda_x) + K_{u_f}(\lambda_m)}\, d\lambda_x \qquad (24)$$

APPENDIX 3. DERIVATION OF $T_f(\lambda)$ FOR A DIODE ARRAY SPECTROPHOTOMETER

Consider a diode array spectrophotometer with panchromatic irradiance $E_0(\lambda_x)$ incident on a sample that contains CDOM but no particles. A certain fraction of $E_0(\lambda_x)$ will be absorbed by the CDOM, fluoresced at a longer wavelength λ_m, and collected by the detector. For a given λ_m, integrating this added irradiance over all possible exciting (i.e. shorter) wavelengths yields a quantity $E_f(\lambda_m)$, and its effect on the apparent transmittance of the sample is $T_f(\lambda_m) = E_f(\lambda_m)/E_0(\lambda_m)$. The fraction of $E_0(\lambda_x)$ that is absorbed by the CDOM is $[1\text{-}10\text{^-}A_{cdom}(\lambda_x)]$ where A is absorbance. The fraction of this absorbed irradiance that is fluoresced at wavelength λ_m is $\eta(\lambda_x,\lambda_m)$, and the fraction of the fluoresced irradiance that is collected by the detector is $\omega/4\pi$, where ω is the solid angle of collection in steradians and the fluorescence is assumed to be an isotropic point source. Putting these factors together and integrating over all λ_x yields $E_f(\lambda_m)$, i.e.

$$E_f(\lambda_m) = \int_{\lambda_x} E_0(\lambda_x)\,(1-10^{-A_{cdom}(\lambda_x)})\,\eta(\lambda_x,\lambda_m)\frac{\omega}{4\pi}\,d\lambda_x \qquad (25)$$

Finally, dividing both sides by $E_0(\lambda_m)$ yields

$$T_f(\lambda_m) = \frac{1}{E_0(\lambda_m)}\frac{\omega}{4\pi}\int_{\lambda_x} E_0(\lambda_x)\,(1-10^{-A_{cdom}(\lambda_x)})\,\eta(\lambda_x,\lambda_m)\,d\lambda_x \qquad (26)$$

APPENDIX 4: DERIVATION OF $T_f(\lambda)$ FOR A REFLECTING TUBE ABSORPTION METER

Consider a reflecting tube absorption meter of pathlength l in meters and collection angle θ_{max} with monochromatic irradiance $E_0(\lambda_x)$ incident on the front end of the sample cylinder which contains a sample with CDOM. A certain fraction of $E_0(\lambda_x)$ will be absorbed by the CDOM, fluoresced at a longer wavelength λ_m, and collected by the detector. Integrating this added irradiance over all emission wavelengths and assuming that the detector has a spectrally flat quantum response yields a quantity $E_f(\lambda_x)$ and its effect on the apparent transmittance of the sample is $T_f(\lambda_x) = E_f(\lambda_x)/E_0(\lambda_x)$. Neglecting the effects of scattering, the fraction of $E_0(\lambda_x)$ remaining at a distance of x meters from the front end of the sample cylinder is $\exp(-a(\lambda_x) \cdot x)$ where a is the total absorption coefficient in m^{-1}. Assuming a homogeneous sample, the fraction of this irradiance that is absorbed by CDOM in the pathlength element dx is $a_{cdom}(\lambda_x) \cdot dx$, and the fraction of this absorbed irradiance that is fluoresced at wavelength λ_m is $\eta(\lambda_x,\lambda_m)$. The fraction of this fluoresced irradiance that can be collected by the detector if no more attenuation takes place is $\omega/4\pi$, where ω is the solid angle of collection in steradians defined by the cone of all photon paths with angles $< \theta_{max}$ from the cylinder axis. However, this fluoresced irradiance will be attenuated along the remaining pathlength (i.e. from x to l) before it reaches the detector end of the sample cylinder. The attenuation factor is approximated by $\exp[-a(\lambda_m) \cdot (l-x)/\mu]$ where μ is the average of $\cos\theta$ for all of the

APPENDIX 4 (Continued)

photons within the cone of detection and θ is the angle the photon path makes with the cylinder axis. Putting all of these factors together and integrating over all λ_m and over the entire pathlength will yield $E_f(\lambda_x)$. For the $\eta(\lambda_x,\lambda_m)$ functions measured in Part 1, the range of λ_m for a given λ_x is from λ_x to 700 nm, so

$$E_f(\lambda_x) = \int_{\lambda_x}^{700} \int_{0}^{l} E_0(\lambda_x)\exp[-a(\lambda_x)x - a(\lambda_m)(l-x)/\mu]a_{cdom}(\lambda_x)\cdot \eta(\lambda_x,\lambda_m)\frac{\omega}{4\pi}\, dx\, d\lambda_m \tag{27}$$

Finally, dividing both sides by $E_0(\lambda_x)$ yields

$$T_f(\lambda_x) = \frac{\omega}{4\pi}\, a_{cdom}(\lambda_x) \int_{\lambda_x}^{700} \int_{0}^{l} \exp[-a(\lambda_x)x - a(\lambda_m)(l-x)/\mu]\cdot \eta(\lambda_x,\lambda_m)\, dx\, d\lambda_m \tag{28}$$